NATIONAL OCEANOGRAPHY CENTRE, SOUTHAMPTON

RESEARCH & CONSULTANCY REPORT No. 1

The impact of surface flux anomalies on the mid-high latitude Atlantic Ocean circulation in HadCM3

J P Grist, S A Josey & B Sinha

2005

RAPID Project – The Role of Air-Sea Forcing in Causing Rapid Changes in the North Atlantic Thermohaline Circulation
Report No. 1

National Oceanography Centre, Southampton
University of Southampton, Waterfront Campus
European Way
Southampton
Hants SO14 3ZH UK

Author contact details:
Tel: +44 (0)23 8059 6175
Fax: +44 (0)23 8059 6204
Email: jyg@noc.soton.ac.uk

DOCUMENT DATA SHEET

AUTHOR

GRIST, J P, JOSEY, S A & SINHA, B

PUBLICATION DATE

2005

TITLE

The impact of surface flux anomalies on the mid-high latitude Atlantic Ocean Circulation in HADCM3.

REFERENCE

Southampton, UK: National Oceanography Centre, Southampton, 19pp. & figs.
(National Oceanography Centre Southampton Research and Consultancy Report, No. 1)
(Unpublished manuscript)

ABSTRACT

Early results from a study of the response of the North Atlantic circulation to anomalous air-sea forcing in the Hadley Centre coupled ocean-atmosphere model (HadCM3) are reported; the study forms part of a Natural Environment Research Council (NERC) Rapid programme project. An analysis of 100 years of the HadCM3 control run indicates that deep convection occurs in the Greenland Sea, the Irminger Basin and the Labrador Sea. However, a composite analysis of mixed layer depth only reveals a clear connection between deep convection and air-sea flux anomalies in the Greenland Sea, and we have focused on this region in our subsequent analysis. Evaluation of the different components of the density flux in the Greenland Sea shows that the net heat flux is a more important influence on surface density than both net evaporation and ice melt. A composite analysis of the ocean circulation was carried out for years with anomalously strong and weak heat loss over the Greenland Sea. Years of strong heat loss are associated with increased Greenland Sea convection and a rapid increase in the southward flow through the Denmark Strait by about 30%. Evidence of more widespread changes in the circulation at mid-high latitudes was also found but we have not yet established whether they are directly linked to the anomalous Greenland Sea forcing.

KEYWORDS

ISSUING ORGANISATION

National Oceanography Centre, Southampton
University of Southampton, Waterfront Campus
European Way
Southampton SO14 3ZH
UK

ABSTRACT

Early results from a study of the response of the North Atlantic circulation to anomalous air-sea forcing in the Hadley Centre coupled ocean-atmosphere model (HadCM3) are reported; the study forms part of a Natural Environment Research Council (NERC) RAPID programme project. An analysis of 100 years of the HadCM3 control run indicates that deep convection occurs in the Greenland Sea, the Irminger Basin and the Labrador Sea. However, a composite analysis of mixed layer depth only reveals a clear connection between deep convection and air-sea flux anomalies in the Greenland Sea, and we have focused on this region in our subsequent analysis. Evaluation of the different components of the density flux in the Greenland Sea shows that the net heat flux is a more important influence on surface density than both net evaporation and ice melt. A composite analysis of the ocean circulation was carried out for years with anomalously strong and weak heat loss over the Greenland Sea. Years of strong heat loss are associated with increased Greenland Sea convection and a rapid increase in the southward flow through the Denmark Strait by about 30%. Evidence of more widespread changes in the circulation at mid-high latitudes was also found but we have not yet established whether they are directly linked to the anomalous Greenland Sea forcing.

1. INTRODUCTION

This report is the first in a series describing results from a Natural Environment Research Council (NERC) RAPID-funded project, which has the primary aim of determining the role of air-sea forcing in causing rapid changes to the North Atlantic Thermohaline Circulation (THC). In the context of the project, 'rapid' refers to changes of the order 20% on decadal to centennial timescales. It has been recognized that variations in the surface fluxes of heat and freshwater have the potential to cause rapid changes in the THC, through their influence on deep convection at high latitudes (Delworth and Greatbatch, 2000). However, the detailed relationship between air-sea flux variability and rapid changes in the circulation has not been established.

In this report we begin to address this issue by presenting an analysis of the output from the control run of the UK Hadley Centre coupled model (HadCM3). Previous studies (e.g. Gordon et al., 2000) have shown that HadCM3 produces a realistic Atlantic THC in terms of both the mean state and variability. The mean Atlantic THC in HadCM3 has similar features to those inferred from estimates using observations (Ganachaud and Wunsch, 2000). In particular, as shown in Fig. 1, the mean meridional streamfunction in the Atlantic has a strength of about 18 Sv. Warm water flows northward in the upper ocean layers, sinks in the Nordic and Labrador Seas and returns south at around 1500m as North Atlantic Deep Water. This cell overlies a weaker cell of about 6 Sv of Antarctic Bottom Water. A weakness of the model is that the Gulf Stream separates from the North American coast too far north compared to observations. Consequences of this include the fact that the North Atlantic Current (NAC) is too zonal and the region of strong SST gradient associated with the NAC is too far north. It should be noted however that these anomalous features of the circulation are common to models of similar resolution (Cooper and Gordon, 2002; Roberts et al., 1996).

Following Vellinga and Wu (2004), we began by calculating summary characteristics of the circulation variability in HadCM3. The variability of the Atlantic THC is depicted in a time series of the annual-mean meridional streamfunction at 45° N in Fig. 2a. The corresponding wavelet transform (Fig. 2b) indicates three different timescales of variability (centennial, multidecadal and interannual). The mechanisms for centennial variability are discussed by Vellinga and Wu (2004) and the interannual variability has been investigated by Dong and Sutton (2002). A number of events with periods of approximately 10-30 years are also evident in Fig. 2b that are rapid changes according to our criteria, and it is this timescale that we have considered thus far. We note that the recent work of Dong and Sutton (2005) into a 25 year oscillation in the HadCM3 THC is relevant to our study. They attributed an acceleration in the THC to a process that involved the accumulation of cold water in the sub-polar gyre during the low phase of the THC. The corresponding acceleration of the sub-polar gyre led to the transport of saline waters into the higher latitudes. The presence of high density surface waters in those regions led to deep convection and a strengthening of the THC. At this stage we have focused on changes in the deep convection regions that occur in response to local surface flux anomalies and will attempt to combine these changes with the response due to advection of remotely forced signals of the type suggested by Dong and Sutton (2005) in subsequent work.

Our approach here has been first to examine air-sea flux variability in Atlantic Ocean deep convection regions and second to study the ocean response to extremes of the surface forcing. The structure of this report is as follows. The model fields used for our analysis are briefly described in Section 2. This is followed by a discussion of the analysis methods in Section 3. Our main results are presented in Section 4. Finally we discuss the implications of the results and summarise our findings in Section 5.

2. MODEL OUTPUT

We have used atmospheric and oceanic output from the control run of HadCM3 and we briefly summarise the main characteristics of the model here. It is a coupled ocean-atmosphere model with sea ice and land surface schemes. There are 19 levels in the atmosphere with a horizontal resolution of 2.5° x 3.75°. The ocean has 20 levels with horizontal resolution of 1.25° x 1.25°. The atmospheric time step is 30 minutes and the atmosphere and ocean components are coupled once per day. The atmospheric component is run with fixed sea surface temperatures (SSTs) through the day and the various forcing fluxes are accumulated each atmospheric model time step. At the end of the day these fluxes are passed to the ocean component. The ocean component is then integrated forward in time. The updated SSTs and sea ice extents are then passed back to the atmospheric model. The control run exhibits a stable climate, without the need for flux corrections for over 1000 years. The model was run with fixed preindustrial greenhouse gases and thus reflects the natural variability of the coupled system (Gordon et al., 2000).

The thousand year control run consists of the nominal years 1850 to 2849. In this study we have been primarily examining a subset of these years (2350 to 2449). The maximum overturning stream function at 45° N for these years only is shown in Fig 2c. It can be seen that there is significant variability in the THC at the timescales of interest during this period. The model output that we have employed was obtained from the British Atmospheric Data Centre (BADC).

3. METHOD

3.1 Identification of Deep Convection Regions

As noted in the Introduction, the areas of primary interest for this study are regions in which deep convection takes place. Deep convection regions in the North Atlantic are identified in Fig. 3 which shows the maximum March mixed layer depth (MLD) for 2350 to 2449. The Labrador Sea (LS), the Irminger Basin (IB) and the Greenland Sea have MLD close to 1000m, which is indicative of deep convection. Boxes defining these regions are also shown in Fig. 3 and their latitude and longitude ranges are indicated in Table 1. The boxes are used to derive area average quantities representative of LS, IB and the Greenland Sea. Note that we have selected two areas for the Greenland Sea, one that surrounds the area of largest MLD (GSA) and one that encompasses the whole Greenland Sea area (GSB). The larger area is included to see if our results are sensitive to the size of area considered. It is also noted that there are mixed layer depths of the

order 800m in the Rockall Trough region, although this is not usually recognized as a region of deep convection.

Time series of the area-averaged net heat flux for GSA, GSB, IB and LS are shown in Fig. 4. Indicated on each time-series are the 10 years of strongest heat loss (STHL) and the 10 years of weakest heat loss (WKHL) for each of the regions. A composite analysis to examine the anomalous MLD for each set of STHL and WKHL years was carried out. This analysis was designed to reveal which of the sites of deep convection were particularly sensitive to extremes of net heat flux forcing.

3.2 Contribution to Surface Density Flux from Different Types of Air-Sea Forcing

The impact of surface fluxes on the density at the ocean surface is quantified by calculating the density flux. Following Schmitt et al. (1989) the total density flux, F_ρ (kg m^{-2} s^{-1}) into the ocean is given by:

$$F_\rho = -\rho\left(\alpha\frac{Q_{Net}}{\rho c_P} - \beta S\frac{E - P}{(1 - S/1000)} + \beta S\frac{I_M}{(1 - S/1000)}\right)$$

Where ρ is the density of water at the sea surface, c_P is the specific heat capacity of water, and S is the sea surface salinity. E-P is the net evaporation through the ocean surface and I_M is the freshwater gained to (or lost from) the surface layer by ice melt (or water freezing). The units of Q_{Net} are W m^{-2} while the units of E-P and I_M are both m s^{-1}. The terms α and β are the thermal expansion and haline contraction coefficients, respectively, which are defined as follows:

$$\alpha = -\frac{1}{\rho}\frac{\partial\rho}{\partial T}$$

$$\beta = \frac{1}{\rho}\frac{\partial\rho}{\partial S}$$

Values for ρ, c_P, α, and β, have been determined using equations summarized by Gill (1982, Appendix 3). Thus the total density flux can be split into the thermal (F_T) components, and two haline components, the net-evaporative density flux (F_S) and the ice melt component (F_{IM}) as follows:

$$F_\rho = F_T + F_S + F_{IM}$$

The different components of the density flux are:

$$F_T = -\left(\alpha\frac{Q_{Net}}{c_P}\right)$$

$$F_S = \rho\left(\beta S\frac{E - P}{(1 - S/1000)}\right)$$

$$F_{IM} = -\rho\left(\beta S\frac{I_M}{(1 - S/1000)}\right)$$

Having calculated the different components to the mean density flux, the correlations between the annual surface density and the components of the density flux for the regions specified earlier were also calculated. To further investigate the nature of the surface forcing, composite fields of the anomalous heat flux and anomalous sea level pressure fields for the STHL and WKHL years were also determined. Note that hereafter we refer to the STHL and WKHL years simply as STHL and WKHL respectively.

3.3 Identifying the Ocean Response to Surface Flux Forcing

To identify the ocean response to extremes in surface forcing we produced composites of ocean currents at 300m, 670m and 1500m for both STHL and WKHL in the Greenland Sea region. We also produced cross-sections of the anomalous flow across a) Denmark Strait, b) Iceland – Scotland passage, c) the 60° N section from Greenland to Scotland (GS60) and d) the 55° N section from Newfoundland to Ireland for lag 0 to +7 years of the STHL composite. The locations of the cross-sections are indicated in Fig. 3. Composites of years leading STHL for a number of relevant variables were also carried out but did not yield significant results in the context of this report.

4. RESULTS

4.1 Extreme Heat Flux Forcing and Mixed Layer Depth Response

In this section we identify years of extreme net heat flux forcing in the North Atlantic and examine the anomalous MLD fields associated with these events. The time series for the net heat flux of the different areas described in Section 3 are shown in Fig 4. The mean and standard deviation for the time series are listed in Table 2 and the correlations between the time series in Table 3.

Considering the Greenland Sea first, the GSA and GSB time series show broadly similar temporal variability. They share 5 of their 10 strongest heat loss years and 5 of the weakest heat loss years and have an r^2 value of 0.71. However, with a standard deviation of 20 W m^{-2} compared to 11 W m^{-2} the variability is greater in GSA than in GSB. This difference may reflect an averaging out of flux anomalies over the larger GSB region. In addition it is noted that in GSA the strong heat loss years are concentrated in 3 distinct clusters whereas in GSB they are more dispersed. The time series for the Labrador Sea and Irminger Basin are not strongly correlated with either the GSA or GSB time series, with values of r^2 that are typically less than 0.1. A slight exception to this is a weak negative correlation ($r = -0.42$, $r^2 = 0.18$) between LS and GSB which is consistent with observations that the North Atlantic Oscillation has an opposite influence on heat exchange in these two regions. Note also, that there is only a weak positive correlation ($r = 0.32$) between the IB and LS time series which might have been expected to be larger given the close proximity of these regions. As regards the mean heat exchange over the period considered,

regions GSA, LS and IB have similar values for the mean net heat flux (-48 W m^{-2}, -40 W m^{-2} and –49 W m^{-2} respectively) which are within the one standard deviation of each other. The mean heat loss of GSB, however, is noticeably stronger (-66 W m^{-2}).

The anomalous MLD for STHL and WKHL conditions for each of the 4 region dependent composites is shown in Fig. 5. GSA and GSB show significantly larger (smaller) MLD, that is an increase (decrease) of up to 91m (97m) and 103m (126m) respectively, associated with STHL (WKHL). This is consistent with deep ocean convection being forced (inhibited) by strong (weak) heat loss events. The deepening of the mixed layer is slightly more to the north in GSB, but in general the ocean response in GSA and GSB is very similar. Therefore to avoid repetition, the GSB results are not discussed further. In contrast, the increase in the MLD in IB and LS associated with the extreme heat loss events over these regions is noticeably smaller than that found for the Greenland Sea regions. This is interesting because observational work (Bacon et al., 2003; Pickart et al., 2002) and studies with HadCM3 and other models (Cooper and Gordon, 2002) suggest that LS and IB are important sites of deepwater formation. It is possible that a greater ocean response is found in more intense heat flux events in other parts of the control run. For the part of the control run considered here the mean heat loss for STHL in LS and IB was 14 W m^{-2} and 11 W m^{-2} less than that in GSB respectively (see Table 3). It is also possible that deep water formation in these regions is driven more by advective processes. These issues will be examined in subsequent work within the project.

Strong (weak) heat loss years over the IB are accompanied by a spatially confined small increase (decrease) in MLD in the region. Specifically in STHL years the maximum increase in the IB MLD is 65m while in the WKHL years the maximum decrease in IB MLD is 49m. It is also of interest that the strong (weak) heat loss years over IB are accompanied by a decrease of up to 81m (increase of up to 78m) in MLD over the Greenland Sea. Although this might suggest that there is a strong anti-correlation in the net heat flux time series of IB and GSA or GSB, Table 2 shows that this is not the case. Indeed only one year is common to STHL of GSA and WKHL of IB and no year is common to STHL of GSB and WKHL of IB. Analysis of the anomalous sea level pressure (SLP) associated with the extreme heat loss events suggests that the heat loss over the Greenland Sea in the IB WKHL years is caused by a different synoptic pattern than that which occurs in GSA STHL years (see Fig. 9 in next section).

For the LS region, strong heat loss years are associated with an increase in the MLD of about 50 m over a relatively small area. This is again accompanied by a decrease in MLD of up to 40 m over parts of the Greenland Sea. It is likely that the apparent relationship between LS and IB net heat loss and the Greenland Sea MLD anomalies is an artifact of the relatively short (100 year) period and the clustering of extreme heat loss years within that period which has the potential to produce spurious relationships due to the small sample of events considered. In the next phase of the project a much longer period of the control run will be examined in order to avoid this problem. However, we are still able to say that in general the response of the MLD to surface forcing in both the Irminger Basin and Labrador Sea in HadCM3 is much weaker than that found over the Greenland Sea. Consequently we have focused on the GSA region for the remainder of the study reported here.

4.2 Air-Sea Forcing and Surface Density Variations

In this section we examine the type of air-sea forcing that is most important for causing changes in the surface density in the 4 study regions. Fields showing the 100 year means and standard deviations of the different types of air-sea forcing; E-P, Q_{Net} and I_M are shown in Fig 6. The strongest heat loss, up to 150 W m^{-2} is found in the Gulf Stream region. Others regions of strong heat loss include the area around Iceland and the northern Greenland Sea. The mean heat loss over the LS and IB regions is smaller, of order 70 W m^{-2}. The strongest variability in the net heat flux occurs over the Greenland Sea with a maximum standard deviation of 44 W m^{-2} compared to 22 W m^{-2} and 21 W m^{-2} in the LS and IB respectively. Considering the freshwater flux, the mean and standard deviation of E-P are relatively moderate in our regions of interest compared to areas further south. The maximum magnitude is a net precipitation of 2.5 ± 0.3 x 10^{-8} m s^{-1} compared to a net evaporation of 7.3 ± 1.3 x 10^{-8} m s^{-1} in the tropical Atlantic (not shown). The remaining I_M term adds freshwater as ice melts or increases surface salinity as ice forms and is confined to the high latitudes. However, it is instructive to see that in the high latitudes the magnitude and variability of freshwater flux from the ice-melt term is substantially greater than that from E-P. Specifically north of 60° N in the Atlantic, the maximum mean net precipitation is 4.1 x 10^{-8} m s^{-1}. This occurs just to the east of the tip of Greenland and the standard deviation there is 0.9 x 10^{-8} m s^{-1}. This compares to the maximum mean input of freshwater of 22.6 x 10^{-8} m s^{-8} from the I_M term. This occurs in the Denmark Strait and the standard deviation there is 7.9 x 10^{-8} m s^{-1}.

Although it is evident from Fig. 6 that I_M is more important at high latitudes than E-P, in order to quantify how important haline forcing is compared to thermal forcing it is necessary to calculate their contributions to the density flux. Fields of the annual mean and standard deviation of the component contributions to the density flux are shown in Fig. 7. It is evident that in our areas of interest, the thermal contribution, F_T, dominates over the two haline terms, F_S, and F_{IM}. This is also evident from Table 4 which shows the area-averaged density fluxes for each region as well as the range of fluxes occurring in each region. It can be seen that in our four regions the area average value of F_T ranges from 9.4 x 10^{-7} kg m^{-2} s^{-1} to 18.6 x 10^{-7} kg m^{-2} s^{-1} while F_S ranges from –3.0 10^{-7} kg m^{-2} s^{-1} to -0.6 x 10^{-7} kg m^{-2} s^{-1}. The opposite signs of the terms indicates that in the mean the thermal flux is acting to increase surface density while the net evaporative flux is acting to decrease the surface density. The area-averaged density fluxes for the ice term are small for both of the Greenland Sea areas. However the range shows that locally the impact can be larger than the thermal flux, in either sense depending on whether ice is melting or forming. The density flux from the ice term in the IB and LS is predominantly from ice melt and thus acts to decrease surface density. In the LS, the area-averaged ice flux term is -6.9 x 10^{-7} kg m^{-2} s^{-1}, which is about two-thirds the magnitude of the thermal term. In the IB, the area-average ice term is about an order of magnitude less than the thermal term. However, locally the term can be as much as -22.0 x 10^{-7} kg m^{-2} s^{-1} compared with local values of up to 31.0 x 10^{-7} kg m^{-2} s^{-1} from the thermal term.

The relative influence of the thermal and haline terms is further illustrated in Fig. 8 which shows the correlation in the GSA region between the annual component density flux anomalies and the density anomalies of the surface layer (which have been calculated directly from the model surface temperature and salinity fields). The anomalies in model surface density and the total surface density flux are strongly correlated, r^2 = 0.77, i.e. 77% of the variability in the

density of the model surface layer can be explained by the variability in the surface density flux. Thus, even though we have not considered other processes such as advection, the results suggest that surface forcing is the primary influence on upper level density variability in the Greenland Sea. The correlation between the model surface density and F_T is slightly stronger, $r^2 = 0.85$, while for F_S it falls to 0.34. In contrast, the correlation between the surface density and the I_M density flux is only 0.06. Because of the dominance of the thermal forcing we will concentrate on describing the impact of extremes in net heat flux on the ocean circulation. It is worth noting here the results of Dong and Sutton (2005). In their study of the HadCM3 control run they found that the density changes which lead to deep convection in the Greenland-Iceland-Norwegian Seas are due primarily to upper ocean salinity changes caused by salinity advection. Our results suggest local heat flux forcing anomalies are also important and further work is required to establish which of these two processes is dominant. We note that the area of deep convection considered by Dong and Sutton (2005) extended form 50° N to 80° N and 45° W to 15° W which is significantly larger than our GSA area, and that this difference in regions considered must also be taken into account.

We further illustrate the type of air-sea forcing associated with upper ocean density changes by plotting fields of the anomalies in net heat flux, sea level pressure and wind speed (Fig. 9) for STHL and WKHL. The figures suggest that the heat flux anomalies in the 4 regions are driven by anomalous surface winds. The anomalous sea level pressure and wind fields associated with GSA and GSB heat loss anomalies are broadly similar (Fig. 9a-d)). That is strong (weak) heat loss over the Greenland Sea is associated with low (high) pressure over the Greenland Sea and high (low) pressure to the east over Greenland and the Labrador Sea. This pressure pattern brings anomalous cold (warm) northerlies (southerlies) over the Greenland Sea thus increasing (decreasing) the heat loss from the ocean to the atmosphere. The anomalous fields associated with IB (Fig. 9e and f) are broadly similar to those associated with LS (Fig. 9g and 9h) due the two regions close proximity to one another. Strong (weak) heat loss over the LS and IB is associated with anomalously low (high) pressure centered near Iceland. This brings anomalously cold, continental (warm, maritime) air from the north-west (south-east). This increases (decreases) the flux of latent and sensible heat to the atmosphere. It is also worth noting that the heat loss anomalies over LS and IB are associated with a sea level pressure anomaly pattern which results in wind forcing and heat loss anomalies of the opposite sign in the Greenland Sea. This may partly explain the weak correlation between heat flux anomalies in IB / LS and mixed layer depth anomalies in the Greenland Sea noted in Section 4.1.

4.3 Ocean Response to Surface Flux Forcing

In this section changes in the ocean circulation associated with the extreme heat flux events that were determined earlier for the GSA region are examined. Composite figures of the anomalous currents at 300m, 670m and 1500m during the STHL and WKHL extreme years are shown in Figs. 10-12. For reference the mean currents at those levels are also shown. The currents at 300m are indicative of the upper branch of the overturning circulation. The key features of the mean flow, Fig. 10a, at 300m are the northward flow of the Gulf Stream and the North Atlantic Current stretching from Cape Hatteras to the Iceland-Scotland Ridge. In the Greenland Sea there is northward flow on the eastern side of the basin and southward flow on the western side.

Through the Denmark Strait flow is mainly southward, but there is also some strong flow northward. This is considered in greater detail later through an analysis of the Denmark Strait cross section. The juxtaposition of these different flows in the Denmark Strait / Irminger Basin region is indicative of the noisy barotropic component in this region in HadCM3. Flow is cyclonic around the LS and then southward along the Newfoundland coast before it meets the North Atlantic Current. The composite field of current anomalies for the STHL years, Fig. 10b, shows coherent changes over large areas of the North Atlantic although it is not clear to what extent these are linked to the change in Greenland Sea forcing. In particular, the northward Gulf Stream flow increases, as does the northward flow though the central and eastern Greenland Sea, while the cyclonic flow around the LS decreases. There is also an increase in the flow through the Denmark Strait, but as just mentioned, the flow here is very noisy. The anomalous currents coincident with WKHL, Fig. 10c, are essentially the opposite of those associated with STHL. The exception to this is that there is no noticeable decrease in the northward flow in the Gulf Stream region.

The circulation at 670m, Fig. 11, is of interest because it is the lowest model depth at which there is flow through the Denmark Strait and the Iceland-Scotland Ridge. The mean flow is similar to that at 300m, the main differences being that at 670m the flow is weaker and there is less evidence of the strong northward and southward flow on the eastern and western edge of the Greenland Sea respectively. The circulation anomalies, Figs. 11b-c, for the STHL and WKHL composites at 670m are qualitatively similar to those found at 300m although reduced in magnitude by about a half. Comparison of Figs. 10 and 11 indicates there is considerable vertical coherence in the ocean response between the 300 and 670 m levels.

The 1500m level in HadCM3 represents the lower limb of the overturning circulation. The flow is predominantly southward, particularly in the band stretching north-east from Cape Hatteras to the UK and in most of the Greenland Sea, see Fig. 12a. Flow around the LS is weakly cyclonic. In the IB the flow is noisy with strong flow both northward and southward. The clearest anomaly associated with the STHL years is a weaker than normal cyclonic flow in the LS, Fig. 12b. There also is an increase in the flow in the IB and near the Newfoundland coast. However, in both these areas the flow is noisy and the increase does not appear to be in one particular direction. The anomalous currents, Fig. 12c, associated with WKHL are typically in the opposite sense to those associated with STHL.

Summarizing the ocean circulation anomalies during STHL (WKHL) years observed in Figs. 10-12, the upper branch of the MOC is stronger (weaker) in the Gulf Stream region and in the Greenland Sea. The flow around the LS is weaker (stronger) down to 1500m. The flow in the Denmark Strait, IB and Newfoundland Coast region is stronger (weaker) but not in a uniform direction. It thus appears that there are circulation anomalies at the same time as the Greenland Sea surface flux anomalies. However, a causal link has not yet been established. We now examine the circulation changes across different sections in detail using various lag intervals. In particular we examine if there is a significant change in flow through the Denmark Strait and the Iceland-Scotland Ridge (ISR). Insight into this issue is obtained by analysis of the cross sections across 55° N from Newfoundland to Ireland (NFIR), 60° N Greenland to Scotland (GS60), the Denmark Strait and the Iceland Scotland Ridge (ISR), the locations of which are all shown in Fig. 3.

The mean meridional flow across NFIR is shown in Fig. 13 for the full 100 year period. The baroclinic flow, Fig. 13a, is mostly northward above 700m and southward below this level.

The exception to this is the western edge of the basin, where the baroclinic flow above 400m is southward. The strongest upper level northward flow is on the eastern edge of the basin where the baroclinic velocities are close to 5 cm s^{-1}. There is some detailed structure to the barotropic flow, Fig.13b, but in general the flow on the eastern side of the basin is northward and the flow on the western side of the basin is southward. The sum of baroclinic and barotropic components, Fig. 13c, shows the southward flow largely confined to the lower levels and the surface on the western side of the basin. The flow over the rest of the section is predominantly northward, with the strongest flow occurring in the top 400m of the eastern edge of the basin. The anomalous total flow at lags of 0 to 7 years relative to the set of STHL years is shown in Fig 14. The initial response in the western sector of the basin is for a weakening of the upper level southward coastal flow and the northward flow immediately to its east while the southward flow on the lower western side of the basin strengthens. These anomalies persist from 0 to 3 years. This is accompanied by a complicated pattern of anomalous flow in the surface layers. This pattern may be due to the near zonal nature of the Gulf Stream flow in this region. From lag 1 year, the southward flow at 2000m on the eastern side (approximately 20° W) of the basin strengthens, becoming strongest after about 5 years, but persisting until at least 7 years.

Given the complex response observed at 55° N, which probably also reflects factors other than the extreme forcing over the Greenland Sea, we now focus on shorter sections closer to the GSA region. The mean meridional flow across GS60 is shown in Fig. 15. The salient features in the total and baroclinic flow include strong (10 cm s^{-1}) northward flow in the upper layers around 10° W and strong (7 cm s^{-1}) southward flow on the western side of the basin below 1500m. Strong (5 cm s^{-1}) southward flow is also evident in the top 400m on the western side of the section. The barotropic flow is similar to that at 55° N in that there tends to be northward flow towards the eastern boundary and southward flow towards the west. The STHL year composites reveal a complex pattern of circulation anomalies, see Fig. 16. At lag 0 the main feature is an anomalously strong southward flow at 2500m depth, 40° W. This anomaly persists until about year 4. Just to the west of this region, from the surface to the lowest layer, at around 3000m the flow is anomalously northward at lag 0 and lag 1. In the middle of the basin, between 500m and 1700m, the flow is anomalously strong in both directions at lag 0. The northward component of this anomaly is only evident until lag 1, whilst the southward component persists through to lag 7. On the eastern side of the basin, at about 10° W, a northward anomaly in the top 400m becomes apparent at a lag of 2 years and persists out to a lag of 7 years. This is accompanied by anomalous southward flow at about 14° W with similar depth and timescale.

The mean flow through Denmark Strait is shown in Fig. 17. As noted earlier the magnitude of the flow through the Strait is quite strong (up to 30 cm s^{-1}, about 3 times stronger than the strongest flow across GS60, note the change in scale between Figs. 15 and 17) and the spatial structure is quite complex, due to the noisy nature of the barotropic flow. The strongest southward flow (i.e. 30 cm s^{-1}) is in the centre of the Strait, at the lower levels. This central region of southward flow is surrounded by two bands of northward flow. There is also a strong southward flow in a band along the coast of Greenland. Using a higher resolution (~35 km) ocean model, forced with NCEP fluxes for 50 years, Zhang et al. (2004) derived a mean Denmark Strait cross-section flow with a simpler structure. In their analysis, the western 80% of the channel is southward flow (the East Greenland Current) while in the remaining part of the cross-section, the upper-eastern segment, there is northward flow which they term the Irminger Current. The

analysis of Zhang et al. (2004) is more consistent with Hansen and Østerhus's (2000) schematic presentation of Nordic Sea exchanges and is indicative of problems with the representation of the flow in HadCM3. The lagged composite analysis of the flow anomalies in the Denmark Strait for the STHL years is shown in Fig 18. There is a major increase in the deep southward flow from 30 to nearly 40 cm s^{-1} at lags of 0 to 1 years which is accompanied by a strengthening of the adjacent northward flow nearer the surface. At lag 2 there appears to be little difference from the mean flow. At lag 3 through lag 7, an anomalous northward flow is evident along the coast of Greenland.

The mean flow through the Iceland Scotland section is shown in Fig. 19. As indicated in Fig. 3, this consists of the meridional flow across an east-west section and the zonal flow across a north–south section. The flow is dominated by a noisy barotropic component. In the mean, the zonal flow is 5 cm s^{-1} to the west (leaving the Greenland Sea). The meridional flow consists mainly of strong (10 cm s^{-1}) northward flow and some weaker flow in both directions. The anomalous flow (Fig. 20) associated with STHL years reveals an increase in the mean exchanges between the Greenland Sea and the Atlantic. The strongest response occurs 3 - 6 years after the surface flux anomalies. An increase in flow out of the Atlantic is seen to occur during this interval through the northward current in the upper layers of the middle part of the section, while an increase in flow into the Atlantic is apparent in the zonal flow adjacent to Iceland.

Summarising the information derived from the cross-section analysis, a complex pattern of circulation anomalies has emerged. The strongest signal is an increase of the flow through the Denmark Strait from 30 to nearly 40 cm s^{-1} at lags of 0 to 1 years which is accompanied by a strengthening of the adjacent northward flow nearer the surface. Given the closeness of the Denmark Strait to the GSA region on which the composites are based it is likely that the changes in the Strait represent a rapid response to extreme Greenland Sea heat flux anomalies. Circulation anomalies are also observed further to the south at 60° N and 55° N, and across the Iceland-Scotland section but further work is required to establish whether these are related to the changes in the Greenland Sea surface forcing.

5. DISCUSSION

This report describes results obtained in the initial phase of a NERC Rapid Climate Change funded project. The analysis thus far has been concerned with the response of the Atlantic Ocean in a 100 year interval from the HadCM3 control run to anomalous surface forcing in regions of deep convection. We find that in the North Atlantic deep convection regions, the net heat flux is the most important of the surface fluxes for changing the surface density and thus influencing deep convection. In contrast, but consistent with the observational analysis of Schmitt et al. (1989), the net evaporation (E-P) has a much smaller effect on surface density at these latitudes. In addition, the influence of sea-ice melt and formation (I_M) on surface density is also small relative to the net heat flux. An exception to this is the Denmark Strait and Irminger Basin (IB) region where I_M makes a significant contribution to surface density changes. It thus appears that the role of I_M should not be neglected in HadCM3 studies of the North Atlantic THC. However, it should be noted that the I_M flux in the Irminger Basin is due to the melting of sea-ice

that has been advected by the East Greenland Current. The amount of sea-ice advection in this region in HadCM3 is greater than is evident from observations.

Our analysis also revealed a clear response in maximum mixed layer depth (MLD), and by implication deep convection, to extremes in the net heat flux in the Greenland Sea. However, a much weaker response to heat flux extremes was observed in both the Labrador Sea and the Irminger Basin. In an earlier analysis of HadCM3, Cooper and Gordon (2000) did find evidence for deep convection in the Labrador Sea and this may reflect stronger heat flux forcing in the period of the control run that they considered or be indicative of a strong role for advective processes which we have not considered here. Observational studies indicate that anomalously large heat fluxes in both the Labrador Sea (Pickart et al., 2002) and the Irminger Basin (Pickart et. al., 2003) can lead to deep convection. The anomalously large heat fluxes are typically caused by the large air-sea temperature difference and enhanced surface wind which form as a result of cold air outbreaks. It may be that the limited spatial resolution in HadCM3 does not capture cold air outbreaks with sufficient intensity to initiate deep convection. The mean heat loss over the Labrador Sea and the Irminger Basin is weaker than that over the Greenland Sea by at least 10 W m^{-2} in the part of the control run considered here.

A composite analysis of changes in the ocean circulation in years of strong (STHL) and weak (WKHL) heat loss over the Greenland Sea has been carried out. The ocean circulation at the time of STHL (WKHL) has a stronger (weaker) circulation in the Gulf Stream region and in the Greenland Sea. The flow around the LS is weaker (stronger) down to 1500m. These changes are consistent with the idea that anomalously strong (weak) heat loss events over the Greenland Sea can lead to a strengthening (weakening) of the North Atlantic THC, but a full causal link has yet to be established. The process by which heat flux anomalies in the Greenland Sea may lead to changes in the ocean circulation has been explored through a lagged analysis of transport through a number of cross sections. A complex pattern of circulation anomalies emerges with the strongest signal being an increase in deep southward flow through the Denmark Strait by about 30 % at the time of the surface flux anomalies which persists with reduced magnitude for several years thereafter. As the Denmark Strait is close to the GSA region on which the composites are based it is likely that increased southward flow represents a rapid response to the extreme Greenland Sea heat flux anomalies. Circulation anomalies are also observed further to the south but further work is needed to determine whether they are related to the changes in the Greenland sea surface forcing. On this point it is worth noting that in the runs of HadCM3 with increasing CO_2, the flow through the Denmark Strait was not strongly correlated with changes in the North Atlantic THC (Wood et al., 1999). However, this may be partly due the model's inadequate representation of dense water overflows across the Greenland-Scotland ridge. Tang and Roberts (2005) have introduced a bottom boundary layer scheme into HadCM3. In their scheme the density of the overflow is conserved more and thus flows southward at greater depths. This may indicate that their modified version of HadCM3 has a stronger connection between the Denmark Strait overflow and the THC overturning strength.

Zhang et al. (2004) and Biastoch et al. (2003) have also considered how air-sea forcing in the Greenland Sea may effect the Denmark Strait exchanges. These studies acknowledge that the strength of the Denmark Strait overflow is correlated with the NAO. However, they indicate that it is the variability of the surface wind, driving the cyclonic circulation around Iceland, rather than the heat flux that is the more important influence on flow through the Denmark Strait. The

anomalous sea level pressure pattern (Fig. 9) that we have found to be associated with the STHL years suggests that the surface winds, as well as the increased heat loss, may contribute to the increased flow through the Denmark Strait. Further work is needed to separate out the relative contributions of these terms. As noted in the Introduction, Dong and Sutton (2005) have found in a recent HadCM3 study an approximately 25 year oscillation in the THC strength in which advective processes play a key role. Their analysis indicated that following a minimum in the overturning circulation, anomalous ocean heat loss strengthens the sub-polar gyre leading to increased advection of more saline waters into the high latitude convection region. These denser waters play a significant role in increased convection and a subsequent strengthening of the THC. We have not considered the contribution from advected density anomalies in the present analysis but plan to do so in subsequent research.

In summary, our initial analysis of HadCM3 has revealed that extreme heat flux anomalies in the Greenland Sea are linked to a rapid increase in the deep southward flow through the Denmark Strait by about 30%. We have also found evidence of more widespread changes in the circulation at mid-high latitudes but we have not yet established whether they are directly linked to the anomalous Greenland Sea forcing. We plan to address this issue in subsequent work in which our analysis will be extended to include anomalies from the full 1000 years of the HadCM3 control run. In addition, we will examine the ocean response from surface forcing anomalies of longer return periods using FORTE, a coarser resolution coupled ocean-atmosphere model.

ACKNOWLEDGEMENTS

The work described in this report has been funded as part of the NERC RAPID directed programme under the project: The Role of Air-Sea Forcing in Causing Rapid Changes in the North Atlantic Thermohaline Circulation, ref NER/T/S/2002/427.

REFERENCES

Bacon, S., W. J. Gould, and Y. L. Jia, 2003: Open-ocean convection in the Irminger Sea. *Geophys., Res. Letters*, **30 (5):** art. no. 1246.

Biastoch, A., and R. H. Kase, 2003: The sensitivity of the Greenland-Scotland Ridge overflow to forcing changes. *J. Phys. Oceanogr.,* **33,** 2307-2319.

Cooper, C. and C. Gordon, 2002: North Atlantic oceanic decadal variability in the Hadley Centre coupled model. *J. Climate*, **15,** 45-72.

Delworth, T. L., and R. J. Greatbatch, 2000: Multidecadal thermohaline circulation variability driven by atmospheric surface flux forcing. *J. Climate,* **13,** 1481-1495.

Dong, B.- W. and R. T. Sutton, 2002: Variability in North Atlantic heat content and heat transport in a coupled ocean-atmosphere GCM. *Climate Dyn.,* **19,** 385-497.

Dong, B.- W. and R. T. Sutton, 2005: Mechanism of decadal thermohaline circulation variability in a coupled ocean-atmosphere GCM. *J. Climate*., **18,** 1117-1145.

Ganachaud. A., and C. Wunsch, 2000: Improved estimates of global ocean circulation, heat transport and mixing from hydrographic data. *Nature,* **408**, 453-457.

Gill, A. E., 1982: *Atmosphere-Ocean Dynamics, Int. Geophys. Ser.,* vol. 30, 662pp, Academic, San Diego, Calif., 1982.

Gordon, C., C. Cooper, C. A. Senior, H. Banks, J. M. Gregory, T. C. Johns, J. F. B. Mitchell, and R. A. Wood, 2000: The simulation of SST, sea ice extents and ocean heat transports in a version of the Hadley Centre coupled model without flux adjustments. *Climate Dyn.*, **16,** 147-168.

Hansen, B., and S. Østerhus, 2000: North Atlantic-Nordic Seas exchanges. *Prog. Oceanogr.*, **45**, 109-208.

Pickart, R. S., M. A. Spall, M. H. Ribergaard, G. W. K. Moore, and R. F. Milliff, 2003: Deep convection in the Irminger Sea forced by the Greenland Tip Jet. *Nature,* **424,** 152-156.

Pickart, R. S., D. J. Torres and R. A. Clarke, 2002: Hydrography of the Labrador Sea during active convection. *J. Phys. Oceanogr.,* **32,** 428-457.

Roberts, M. J., R. Marsh, A. L. New, and R. A. Wood, 1996: An intercomparison of a Bryan-Cox type ocean model and an isopycnic ocean model. Part I: The subpolar gyre and high-latitude processes. *J. Phys. Oceanogr.,* **26,** 1495-1527.

Schmitt, F. W., P. S. Bogden and C. E. Dorman, 1989: Evaporation minus precipitation and density fluxes for the North Atlantic, *J. Phys. Oceanogr.,* **19,** 1208-1221.

Tang, Y. M. and M. J. Roberts, 2005: The impact of a bottom boundary layer scheme on the North Atlantic Ocean in a global coupled model. *J. Phys. Oceanogr.,* **35,** 202-217.

Vellinga, M. and P. Wu. 2004: Low-latitude freshwater influence on centennial variability of the Atlantic thermohaline circulation. *J. Climate*, **17,** 4498–4511.

Von Storch, H. V, and F. W. Zwiers, 1999: *Statistical Analysis in Climate Research*. Cambridge University Press, 1999.

Wood, R. A., A. B. Keen, J. F. B. Mitchell, and J. M. Wood, 1999: Changing spatial structure of the thermohaline circulation in response to atmospheric CO_2 forcing in a climate model. *Nature,* **399,** 572-575.

Zhang. J., M. Stele, D. A. Rothrock, and R. W. Lindsay, 2000: Increasing exchanges at Greenland Scotland Ridge and their links with the North Atlantic Oscillation and Artic Sea ice. *Geophys, Res. Letters*, **31,** L0937, doi:10.1029/2003GL019304.

TABLES

Region	Longitude ranges	Latitude ranges
GSA	16.25º W to 7.5º E	70.625º N to 76.875º N
GSB	31.25º W to 25.0º E	66.875º N to 84.375º N
IB	37.5º W to 26.5º W	59.375º N to 64.374º N
LS	57.5º W to 51.25º W	58.125º N to 60.625º N

Table 1. Latitude and longitude ranges of the 4 areas of ocean convection identified in the study.

Region	2350-2449	STHL	WKHL
GSA	-48 (± 20)	-86 (± 8)	-16 (± 5)
GSB	-66 (± 11)	-82 (± 3)	-48 (± 3)
IB	-49 (± 12)	-71 (± 8)	-31 (± 3)
LS	-40 (± 15)	-68 (± 7)	-16 (± 6)

Table 2. Area-averaged mean net heat flux (W m^{-2}) for the 4 convective regions for a) 2350-2449, b) the 10 strongest heat loss years (STHL) and c) the 10 weakest heat loss years (WKHL). The standard deviations are shown in parenthesis.

Region	GSA	GSB	IB	LS
GSA	1.00 (1.00)	0.84 (0.71)	-0.10 (0.01)	-0.26 (0.07))
GSB	-	1.00 (1.00)	-0.18 (0.03)	-0.42 (0.18)
IB	-	-	1.00 (1.00)	0.32 (0.10)
LS	-	-	-	1.00 (1.00)

Table 3. Correlations between pairs of time series of the area averaged net heat flux for the 4 regions. Numbers shown are the correlation coefficient, r, with the coefficient of determination, r^2 in parenthesis.

Region	F_ρ	F_T	F_S	F_{IM}
GSA	8.4 (-6.4 to 26.2)	9.5 (0.3 to 27.3)	-1.3 (-2.8 to 0.1)	0.2 (-5.9 to 14.4)
GSB	15.9 (-56.6 to 55.7)	18.6 (-0.6 to 55.7)	-0.6 (-5.5 to 2.3)	-2.1 (-55.9 to 35.1)
IB	12.8 (-19.3 to 29.0)	17.9 (9.4 to 31.0)	-3.0 (-7.0 to –0.8)	-2.1 (-22.0 to 0.1)
LS	0.1 (-15.6 to 14.9)	9.4 (3.8 to 16.6)	-2.4 (-3.2 to –1.2)	-6.9 (-17.3 to 0.1)

Table 4. Area-averaged density fluxes (10^{-7} kg m^{-2} s^{-1}) for the 4 regions. The range of fluxes within each region are indicated in the parenthesis.

FIGURE CAPTIONS

Fig. 1. Zonally averaged Atlantic meridional overturning streamfunction (Sv), mean for HadCM3 model years 2350-2449.

Fig. 2. a) Time series of the maximum values of the annual-mean zonally averaged meridional streamfunction (Sv) in the Atlantic at 45° N, for years 1850-2849 on the control run. b) The natural log of the wavelet power spectrum of a) using a Morlet wavelet. The contours enclose parts of the time-frequency domain where wavelet power exceeds that of a red-noise process with 95% confidence. The curves at the extremes of the time domain denote the 'Cone of Influence' where edge effects are important. c) Time series of the maximum values of the annual-mean zonally averaged meridional streamfunction (Sv) in the Atlantic at 45° N, for years 2350-2449.

Fig. 3. Map showing maximum mixed layer depth (m) for March 2350-2449. Also indicated are the areas of interest for surface forcing. Small Greenland Sea box is GSA, the large Greenland Sea box is GSB, Irminger Basin (IB) and Labrador Sea (LS). Dotted lines indicate analysed cross-sections; Denmark Strait (DMST), Greenland to Scotland (GS60) and Newfoundland to Ireland (NFIR). Grey line is the Iceland-Scotland Ridge (ISR) which was also considered.

Fig. 4. Time series of area average net heat flux (W m^{-2}) for a) GSA, b) GSB, c) IB and d) LS. Green crosses denote the 10 years of weakest heat loss (WKHL) and the red crosses indicate the 10 years of strongest heat loss (STHL).

Fig. 5. Anomalous MLD (m) for composites of STHL and WKHL years in the 4 regions studied a) GSA STHL, b) GSA WKHL, c) GSB STHL, d) GSB WKHL, e) IB STHL, f) IB WKHL, g) LS STHL and h) LS WKHL. The black contour delineates differences from the 100 year mean, which are significant at the 99 % level, using a Student's T test without assuming the samples have equal variance. (von Storch and Zwiers, 1999, section 6.6.5).

Fig. 6. Annual mean and standard deviations (for the period 2350-2449) of air-sea forcing in the North Atlantic a) Q_{Net} (W m^{-2}) – mean b) Q_{Net} (W m^{-2}) – standard deviation, c) E-P (m s^{-1}) - mean, d) E-P (m s^{-1}) – standard deviation, e) I_M (m s^{-1}) – mean f) I_M (m s^{-1}) – standard deviation.

Fig. 7. Annual mean and standard deviations (for the period 2350-2449) of the three components of the surface density flux in the North Atlantic: a) F_T – mean b) F_T – standard deviation, c) F_S - mean, d) F_S – standard deviation, e) F_{IM} – mean f) F_{IM} – standard deviation. Units are Kg m^{-2} s^{-1}.

Fig. 8. Scatter plots showing correlations between surface density anomaly in GSA and anomalies of a) total surface density flux, b) thermal density flux, c) haline density flux and d) Ice-Melt density flux.

Fig. 9. Anomalous net heat flux (W m^{-2}) for a) GSA STHL, b) GSA WKHL, c) GSB STHL, d) GSB WKHL, e) IB STHL, f) IB WKHL, g) LS STHL and h) LS WKHL. Contours are anomalous sea level pressure (hPa). Solid lines are positive anomalies and the zero line, dashed lines are negative anomalies. The interval is 0.4 hPa. Arrows show the corresponding wind velocity anomalies.

Fig. 10. HadCM3 300m layer currents (cm s^{-1}) a) mean (2350-2449), b) anomalous flow for STHL (GSA) and c) anomalous flow for WKHL (GSA).

Fig. 11. HadCM3 670m layer currents (cm s^{-1}) a) mean (2350-2449), b) anomalous flow for STHL and c) anomalous flow for WKHL.

Fig. 12. HadCM3 1500m layer currents (cm s^{-1}) a) mean (2350-2449), b) anomalous flow for STHL and c) anomalous flow for WKHL.

Fig. 13. Mean meridional flow (cm s^{-1}) across the 55° N, Newfoundland to Ireland section (NFIR) for a) baroclinic flow, b) barotropic flow and c) total flow, for the period 2350-2449.

Fig. 14. Anomalous total flow (cm s^{-1}) across 55° N, Newfoundland to Ireland (NFIR) at lags of 0 to 7 years relative to the set of STHL years.

Fig. 15. Mean meridional flow (cm s^{-1}) across the 60° N, Greenland to Scotland section (GS60) for a) baroclinic flow, b) barotropic flow and c) total flow, for the period 2350-2449.

Fig. 16. Anomalous total flow (cm s^{-1}) across 60° N, Greenland to Scotland (GS60) at lags of 0 to 7 years relative to the set of STHL years.

Fig. 17. Mean meridional flow (cm s^{-1}) across the Denmark Strait section (DMST) for a) baroclinic flow, b) barotropic flow and c) total flow, for the period 2350-2449.

Fig. 18. Anomalous total flow (cm s^{-1}) across the Denmark Strait (DMST) at lags of 0 to 7 years relative to the set of STHL years.

Fig. 19. Mean meridional flow (cm s^{-1}) across the Iceland Scotland Ridge (ISR) section for a) baroclinic flow, b) barotropic flow and c) total flow, for the period 2350-2449.

Fig. 20. Anomalous total flow (cm s^{-1}) across the Iceland Scotland Ridge (ISR) at lags 0 to 7 years relative to the set of STHL years.

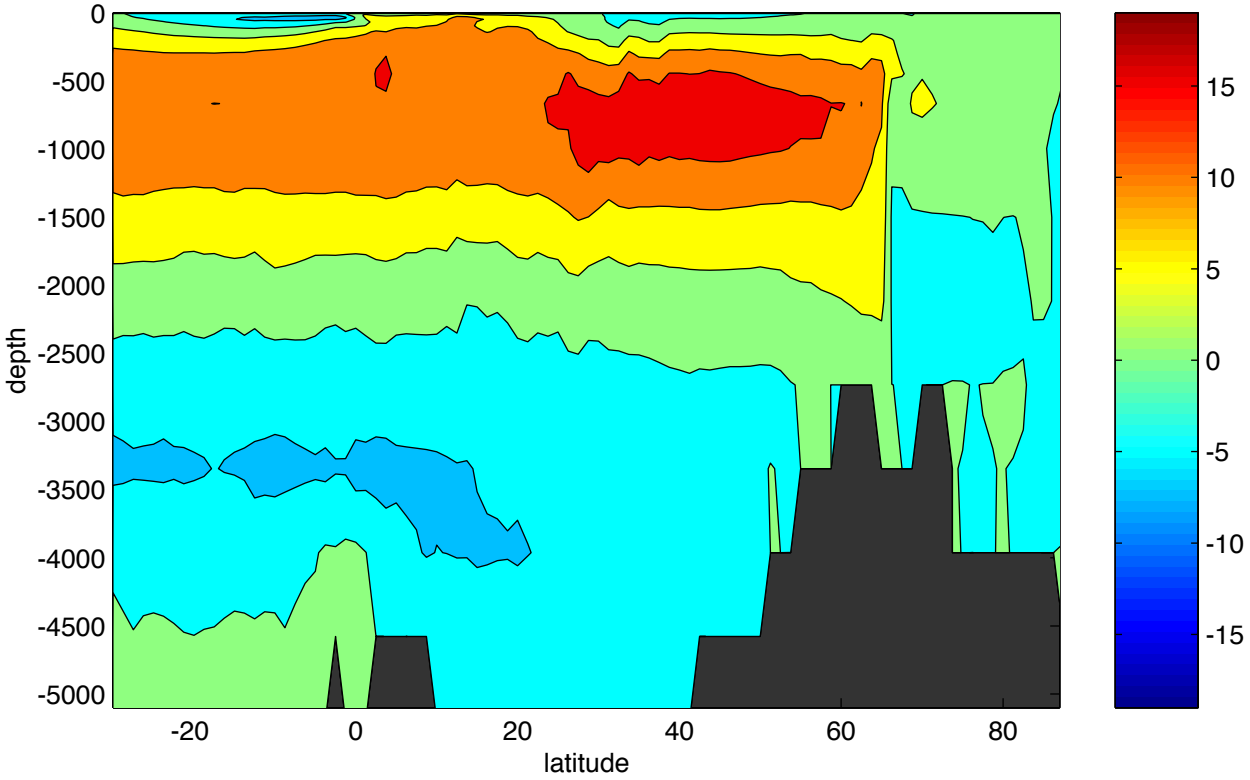

Fig. 1. Zonally averaged Atlantic meridional overturning streamfunction (Sv), mean for HadCM3 model years 2350-2449.

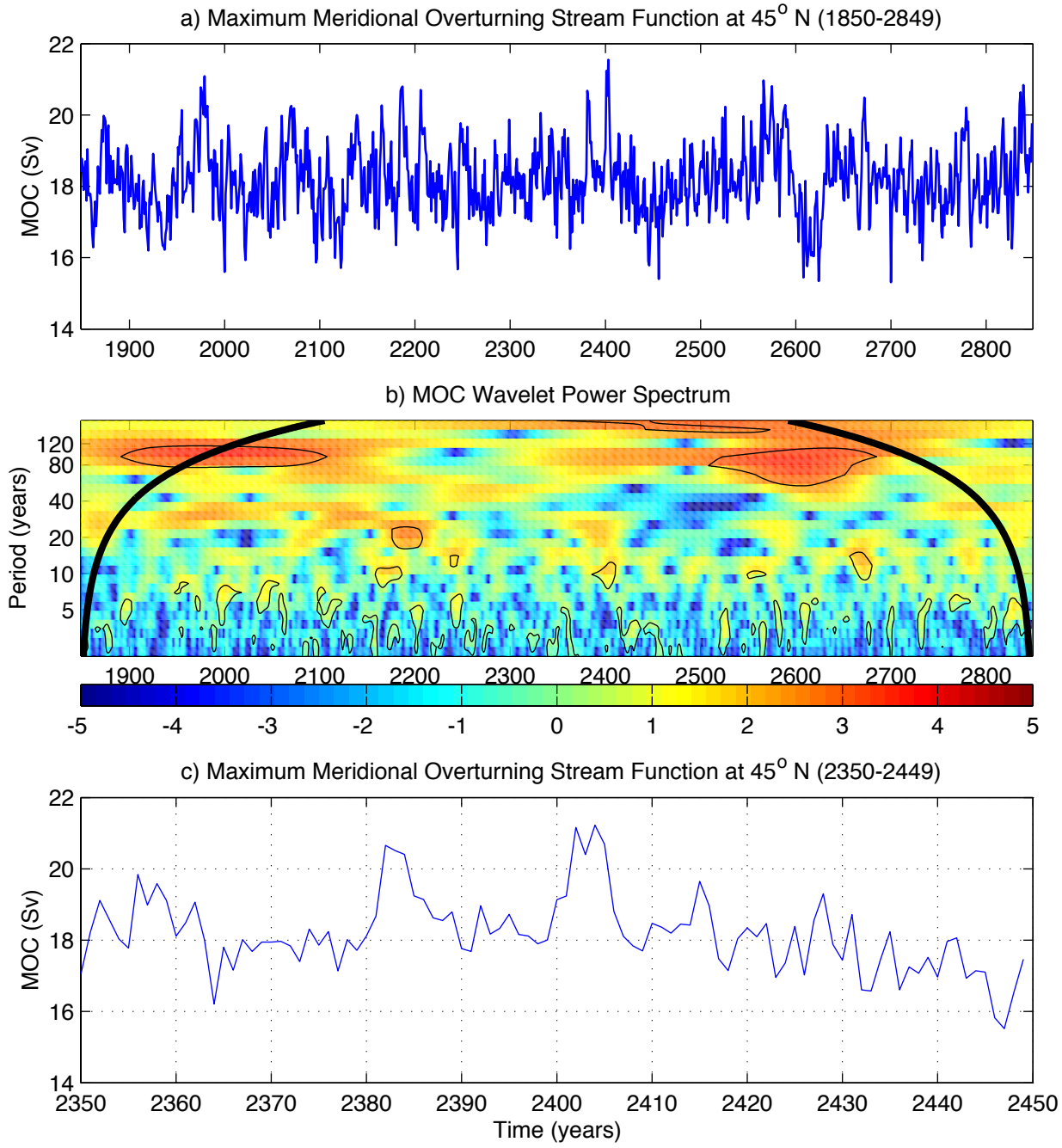

Fig. 2. a) Time series of the maximum values of the annual-mean zonally averaged meridional streamfunction (Sv) in the Atlantic at 45° N, for years 1850-2849 of the control run. b) The natural log of the wavelet power spectrum of a) using a Morlet wavelet. The contours enclose parts of the time-frequency domain, where wavelet power exceeds that of a red-noise process with 95 % confidence. The curves at the extremes of the time domain denote the "Cone of Influence" where edge effects are important. c) Time series of the maximum values of the annual-mean zonally averaged meridional streamfunction (Sv) in the Atlantic at 45° N, for years 2350-2449.

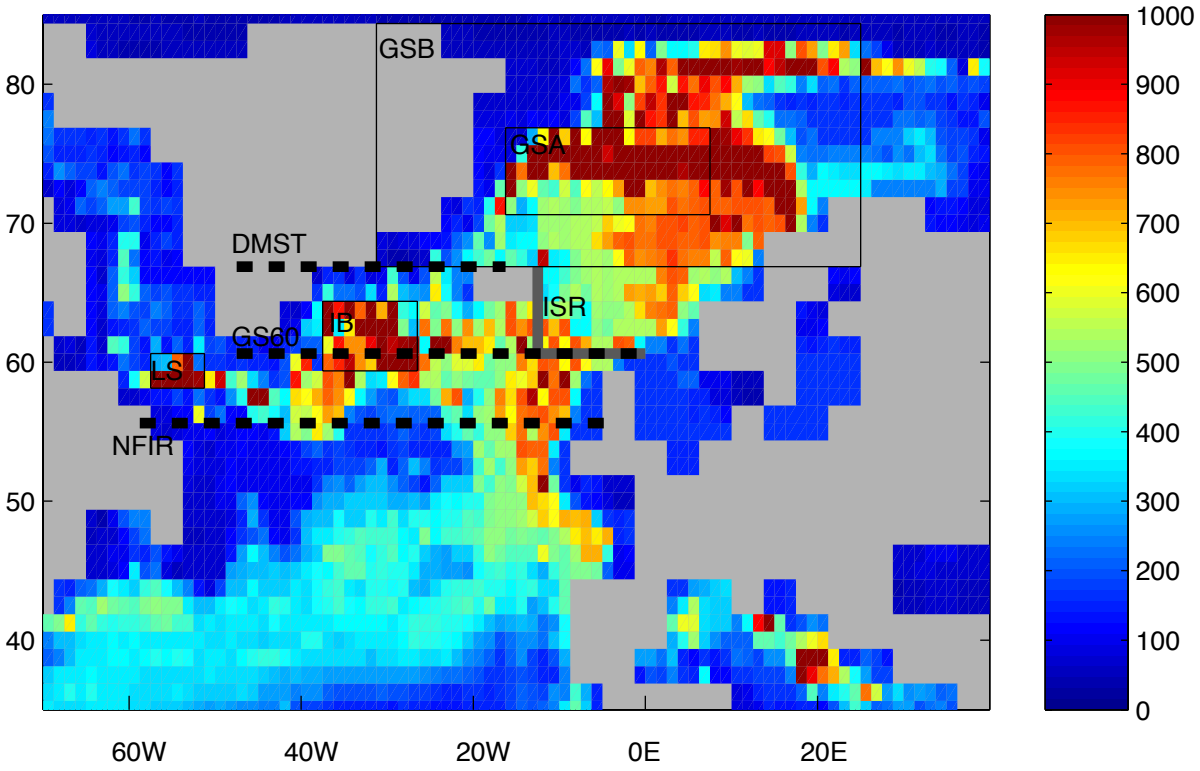

Fig. 3. Map showing maximum mixed layer depth (m) for March 2350-2449. Also indicated are the areas of interest for surface forcing. Small Greenland Sea box is GSA, the large Greenland Sea box is GSB, Irminger Basin (IB) and Labrador Sea (LS). Dotted lines indicate analysed cross-sections; Denmark Strait (DMST), Greenland to Scotland (GS60) and Newfoundland to Ireland (NFIR). Grey line is the Iceland-Scotland ridge (ISR) which was also considered.

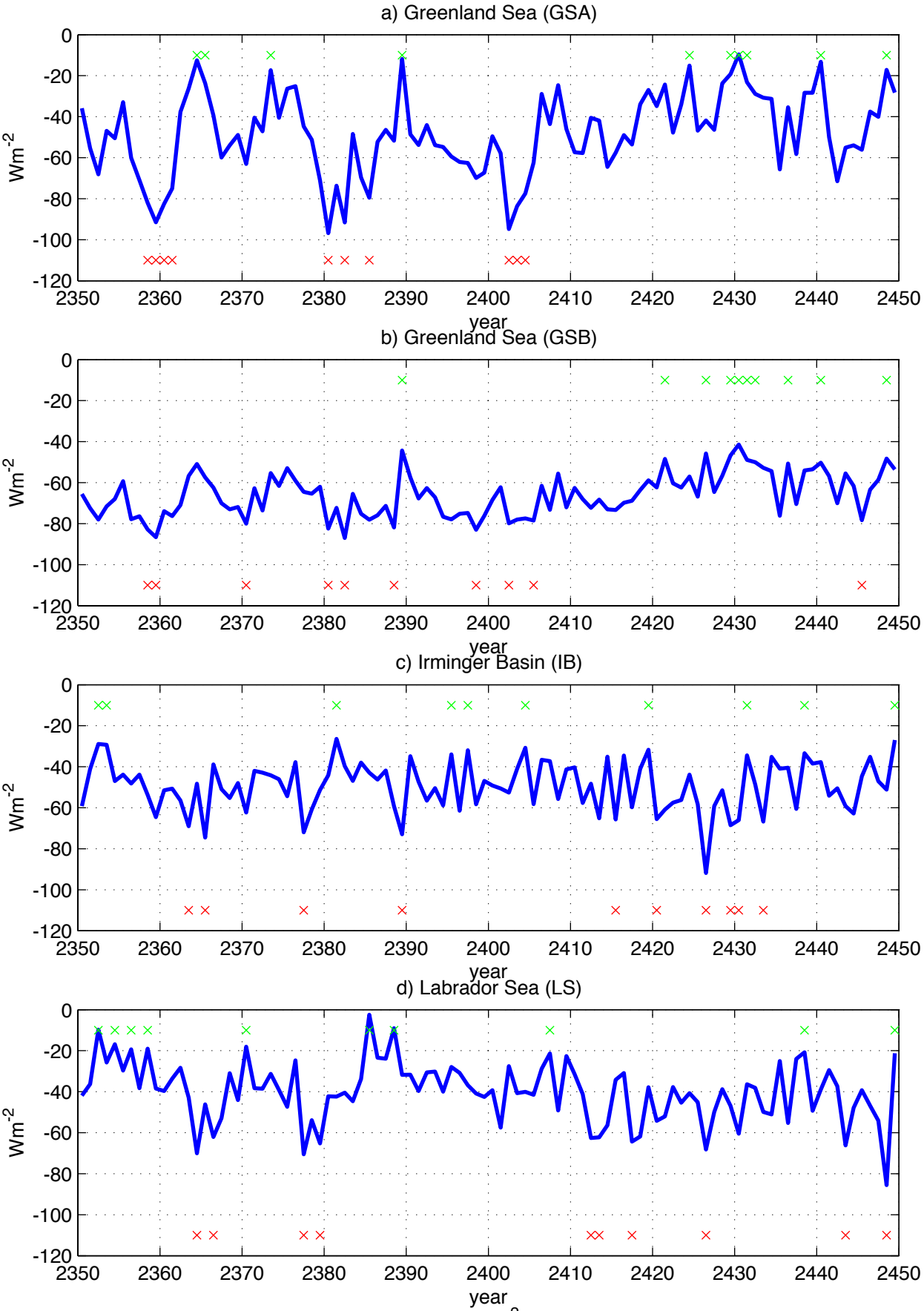

Fig. 4. Time series of area average net heat flux (W m^{-2}) for a) GSA, b) GSB, c) IB and d) LS. Green crosses denote the 10 years of weakest heat loss (WKHL) and the red crosses indicate the 10 years 10 years of strongest heat loss (STHL).

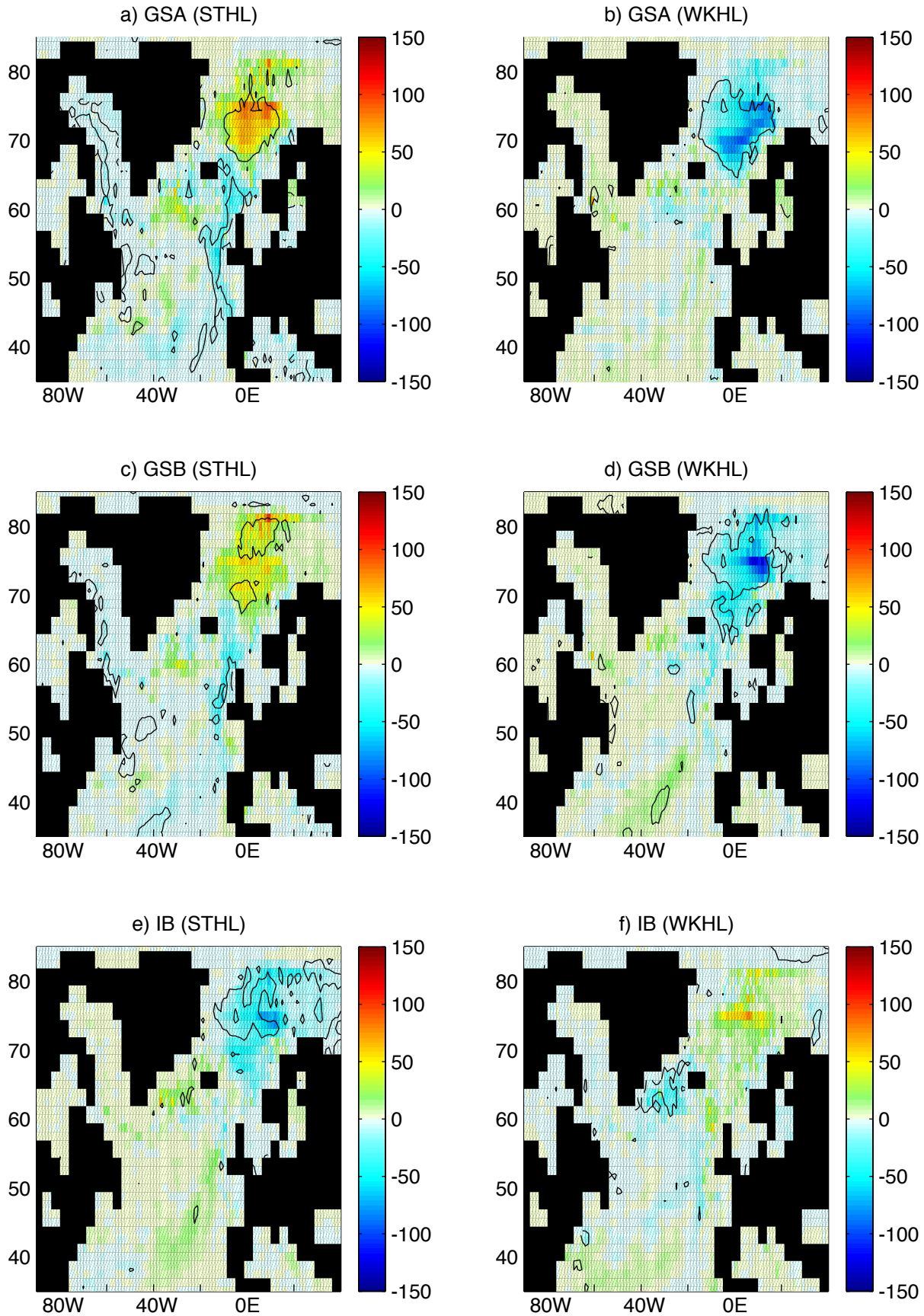

Fig. 5. Anomalous MLD (m) for composites of STHL and WKHL years in the 4 regions studied a) GSA STHL, b) GSA WKHL, c) GSB STHL, d) GSB WKHL, e) IB STHL and f) IB WKHL. The black contour delineates differences from the 100 year mean, which are significant at the 99 % level, using a Students T test without assuming the samples have equal variance. (von Storch and Zwiers, 1999, section 6.6.5.)

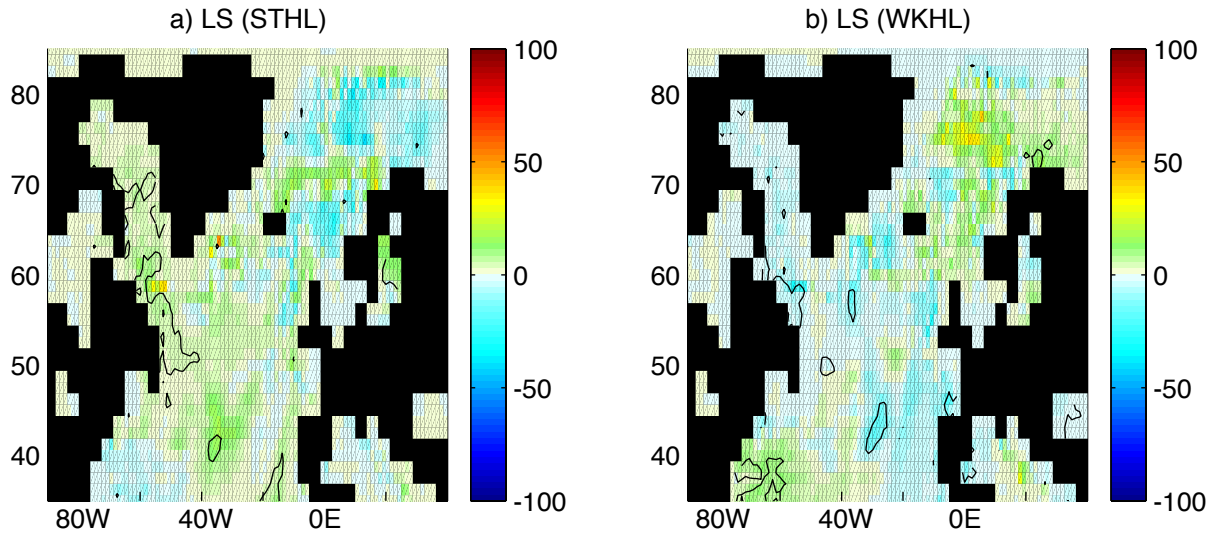

Fig. 5. Anomalous MLD (m) for composites of STHL and WKHL years in the 4 regions studied g) LS STHL, and h) LS WKHL. The black contour delineates differences from the 100 year mean, which are significant at the 99 % level, using a Students T test without assuming the samples have equal variance. (von Storch and Zwiers, 1999, section 6.6.5.)

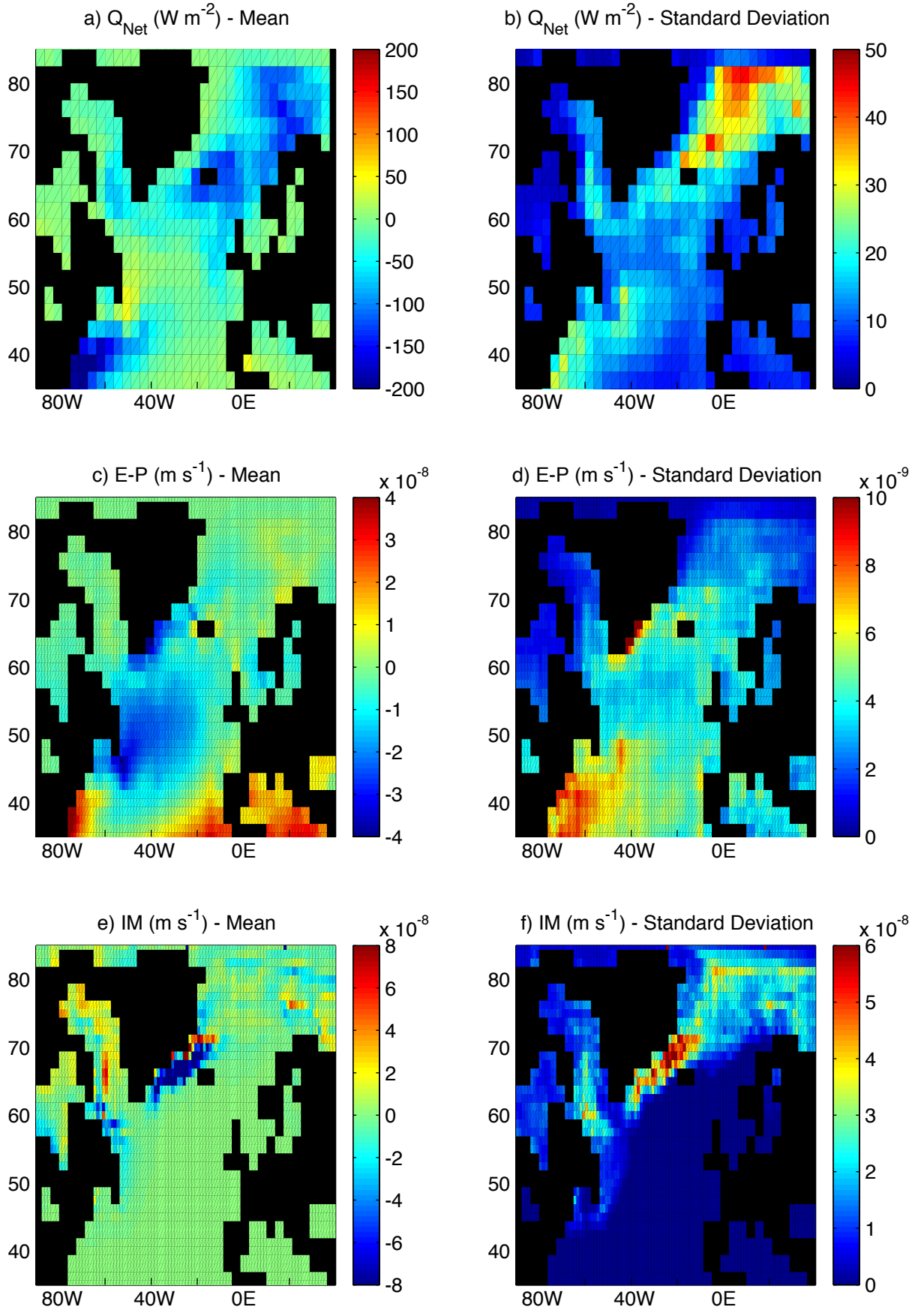

Fig. 6. Annual mean and standard deviations (for the period 2350-2449) of air-sea forcing in the North Atlantic a) Q_{Net} (W m^{-2}) - mean, b) Q_{Net} (W m^{-2}) - standard deviation, c) E-P (m s^{-1}) - mean, d) E-P (m s^{-1}) - standard deviation, e) IM (m s^{-1}) - mean, f) IM (m s^{-1}) - standard deviation.

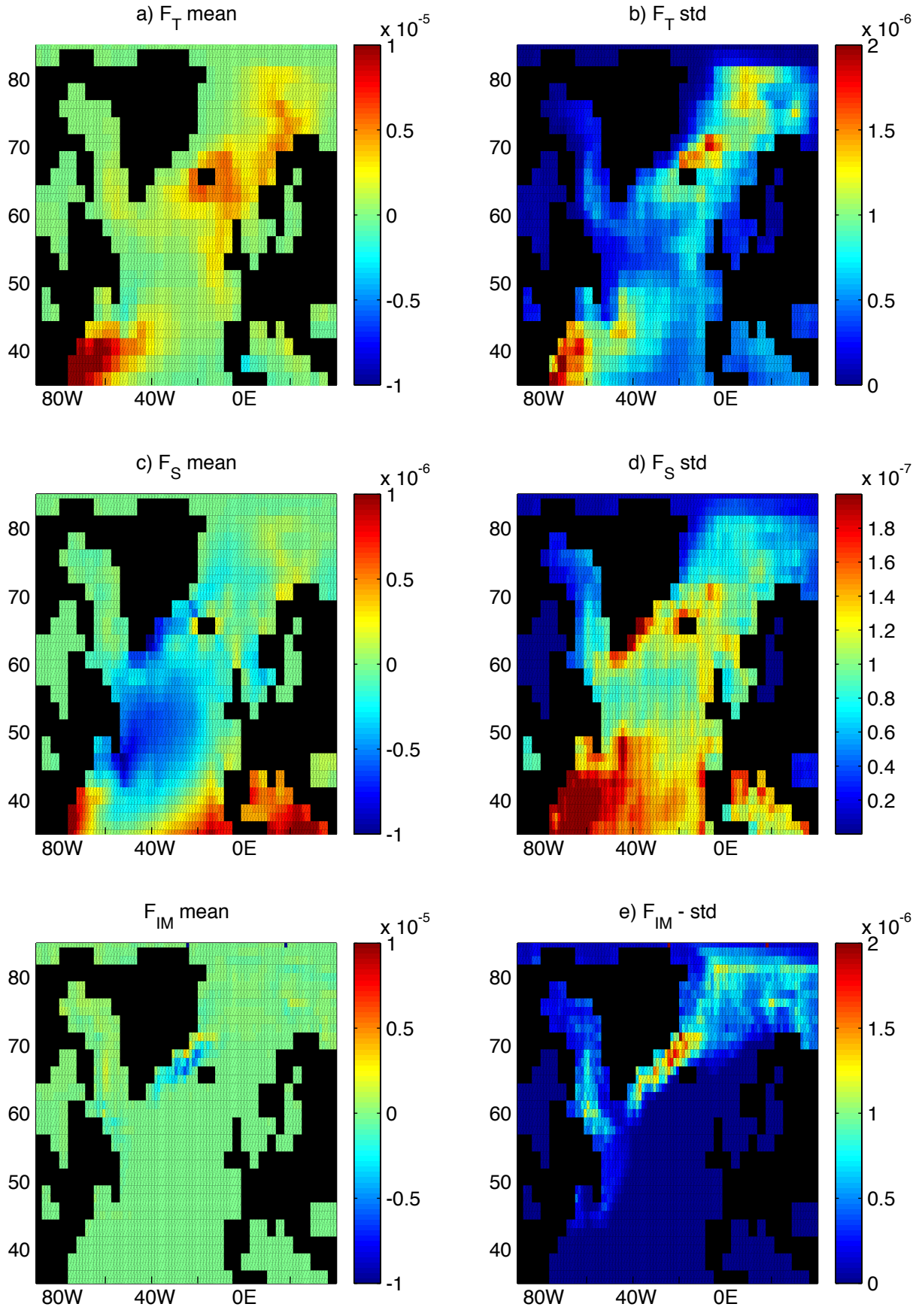

Fig. 7. Annual mean and standard deviations (for the period 2350-2449) of the three components of the surface density flux in the North Atlantic: a) F_T - mean, b) F_T - standard deviation, c) F_S - mean, d) F_S - standard deviation, e) F_{IM} - mean and f) F_{IM} - standard deviation. Units are Kg m^{-2} s^{-1}.

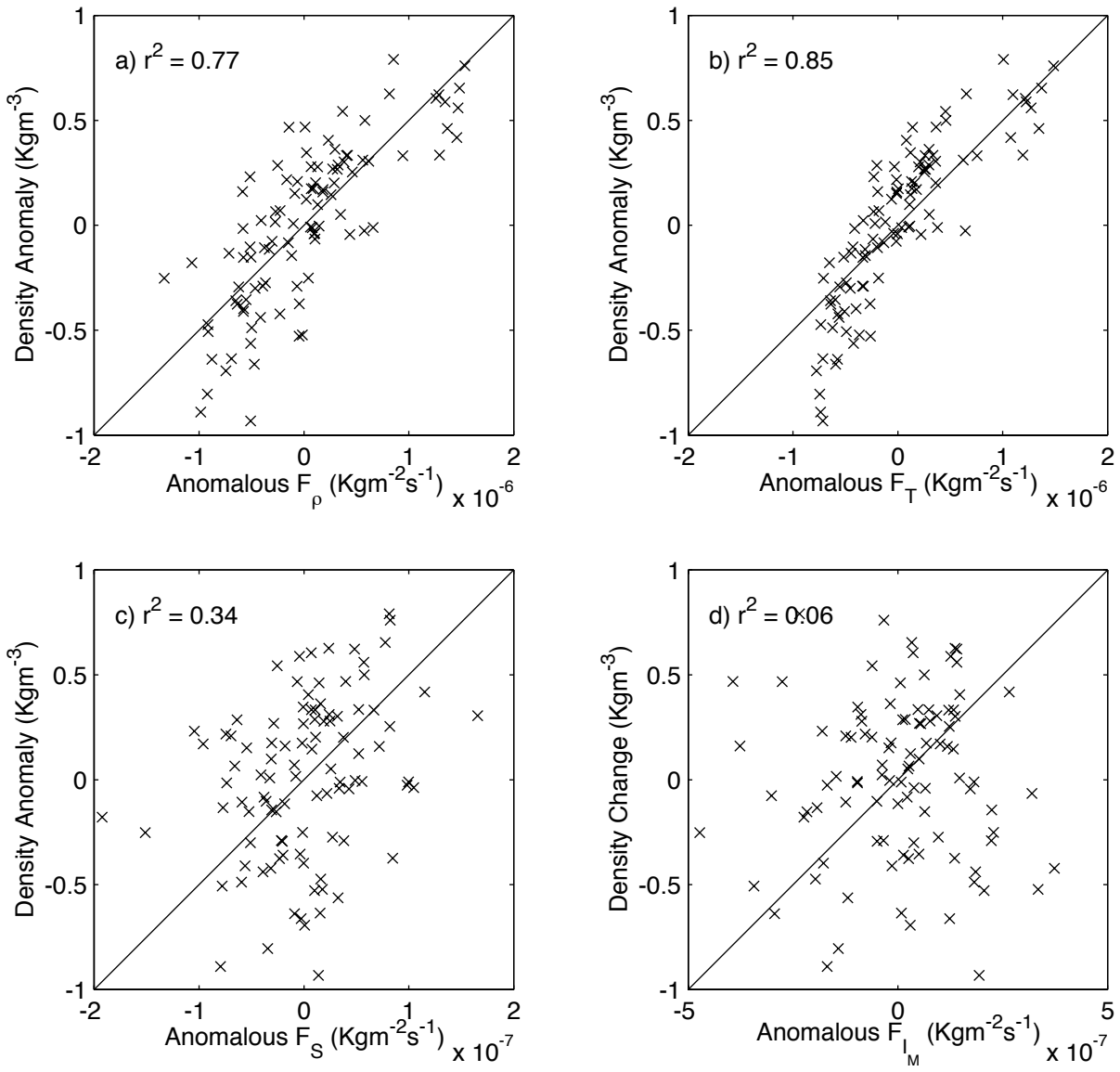

Fig. 8. Scatter plots showing correlations between surface density anomaly in GSA and anomalies of a) total surface density flux, b) thermal density flux, c) haline density flux and d) Ice-Melt density flux.

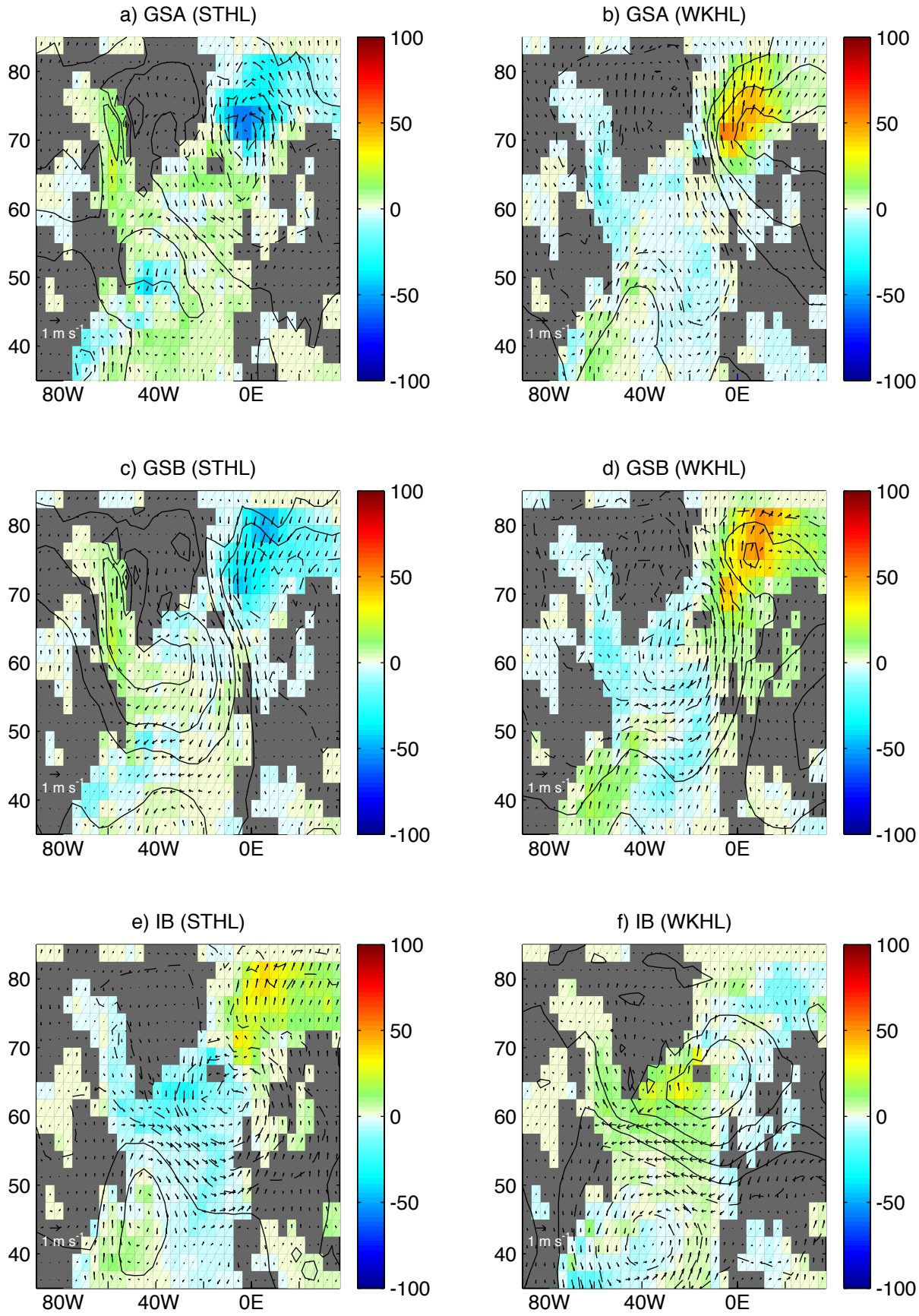

Fig. 9. Anomalous net heat flux (W m^{-2}) for a) GSA STHL, b) GSA WKHL, c) GSB STHL, d) GSB WKHL, e) IB STHL and f) IB WKHL. Contours are anomalous sea level pressure (hPa). Solid lines are positive anomalies and the zero line, dashed lines are negative anomalies. The interval is 0.4 hPa. Arrows show the corresonding wind velocity anomalies.

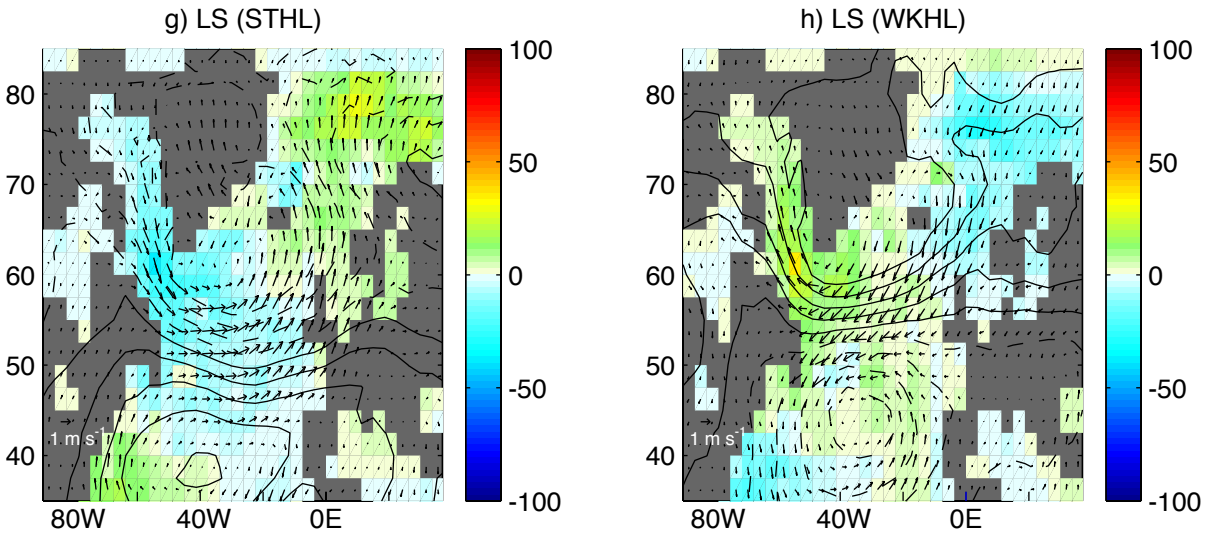

Fig. 9. Anomalous net heat flux (W m^{-2}) for g) LS STHL and h) LS WKHL. Contours are anomalous sea level pressure (hPa). Solid lines are positive anomalies and the zero line, dashed lines are negative anomalies. The interval is 0.4 hPa. Arrows show the corresponding wind velocity anomalies.

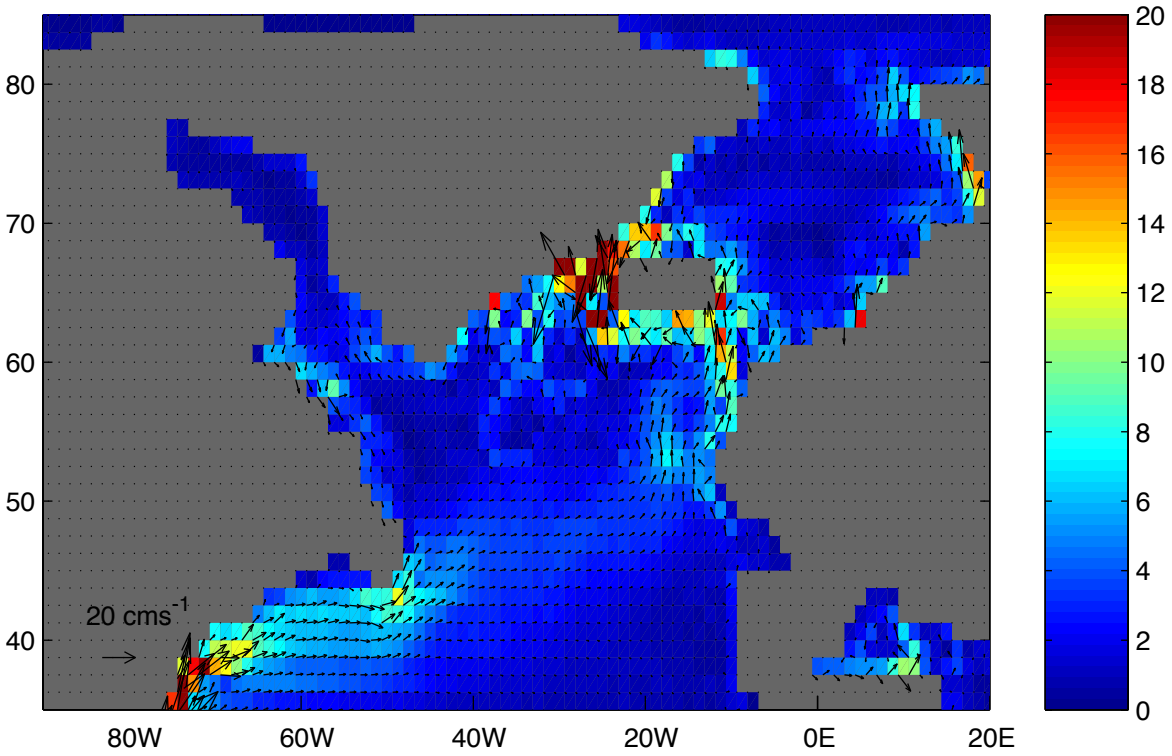

Fig. 10a. HadCM3 300m layer currents (cm s^{-1}) - mean (2350-2449).

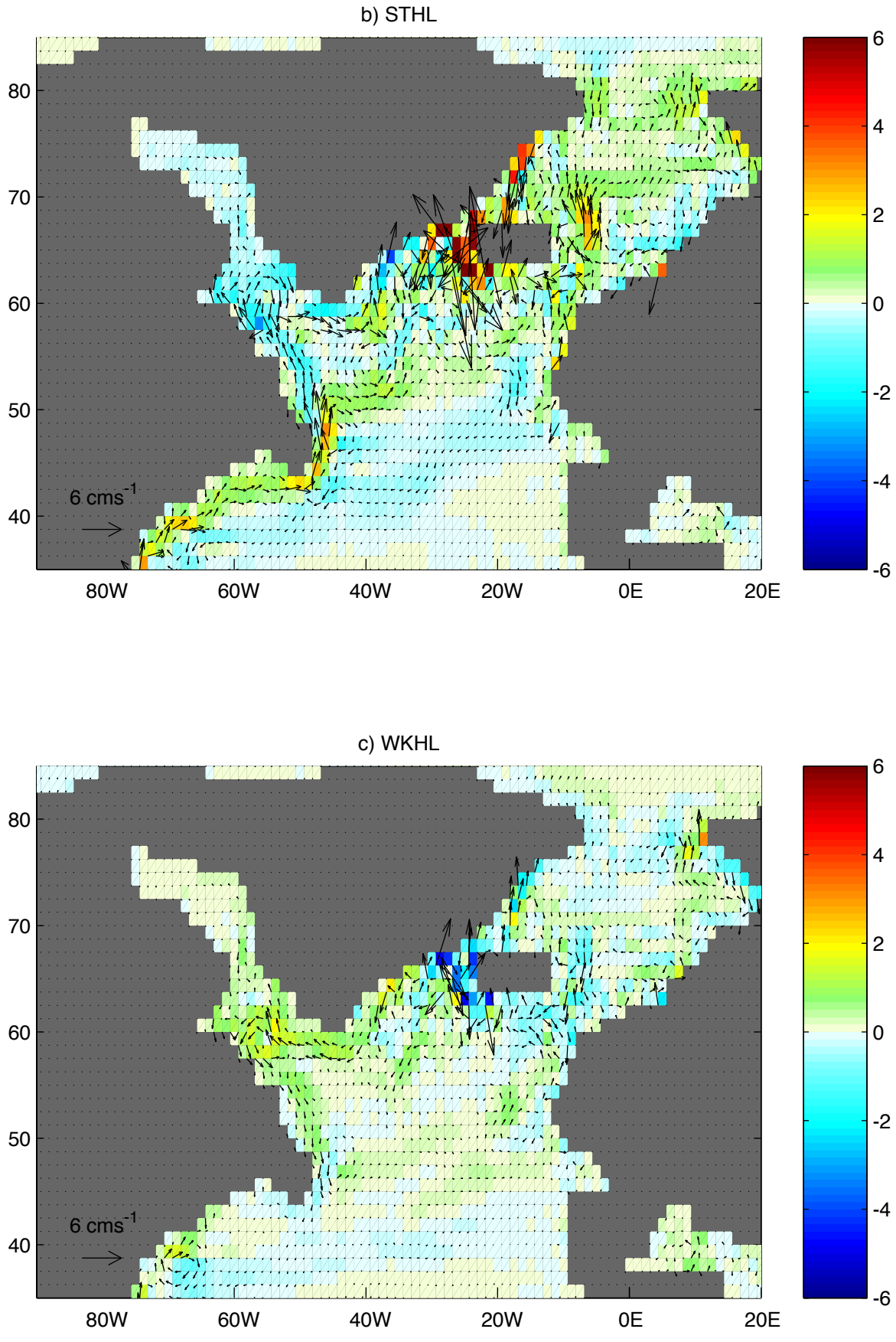

Fig. 10. HadCM3 300m layer currents (cm s^{-1}), b) anomalous flow for STHL (GSA) and c) anomalous flow for WKHL (GSA).

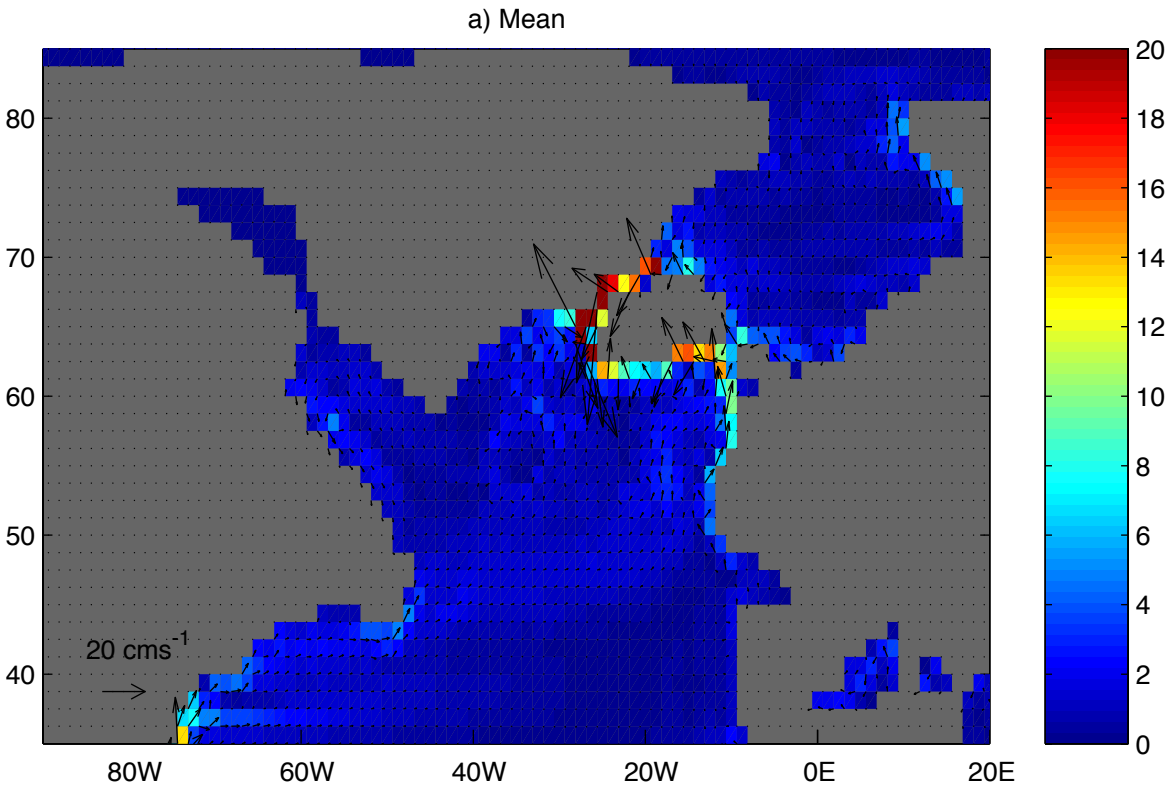

Fig. 11a. HadCM3 670m layer currents (cm s^{-1}) - mean (2350-2449).

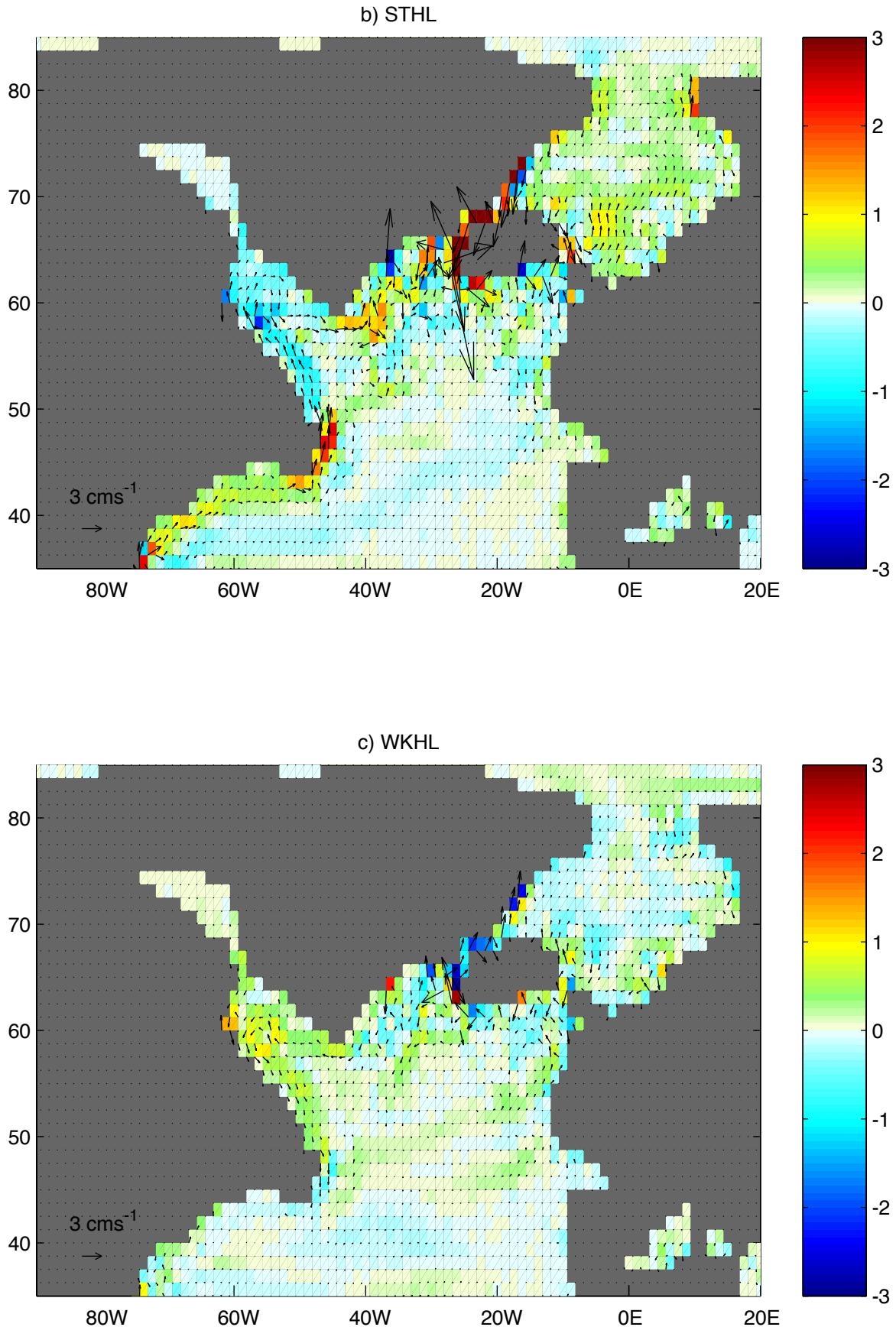

Fig. 11. HadCM3 670m layer currents (cm s^{-1}), b) anomalous flow for STHL and c) anomalous flow for WKHL.

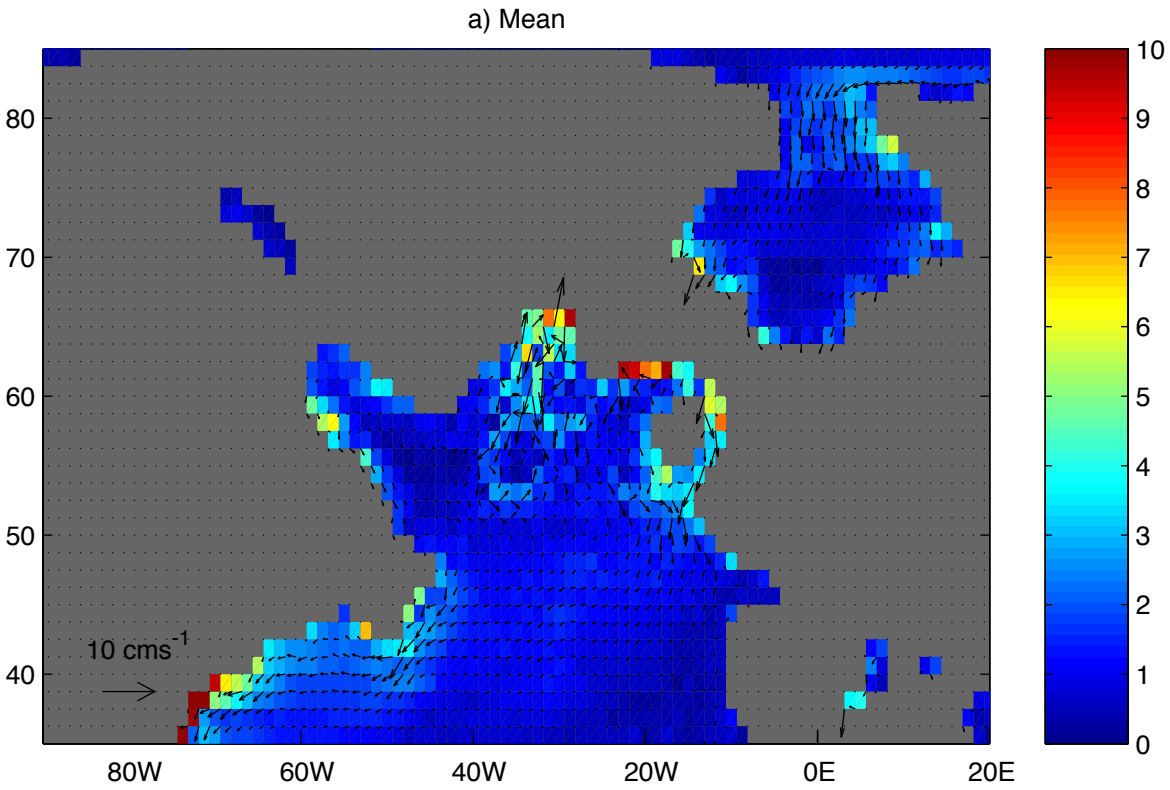

Fig. 12a. HadCM3 1500m layer currents (cm s^{-1}) - mean (2350-2449).

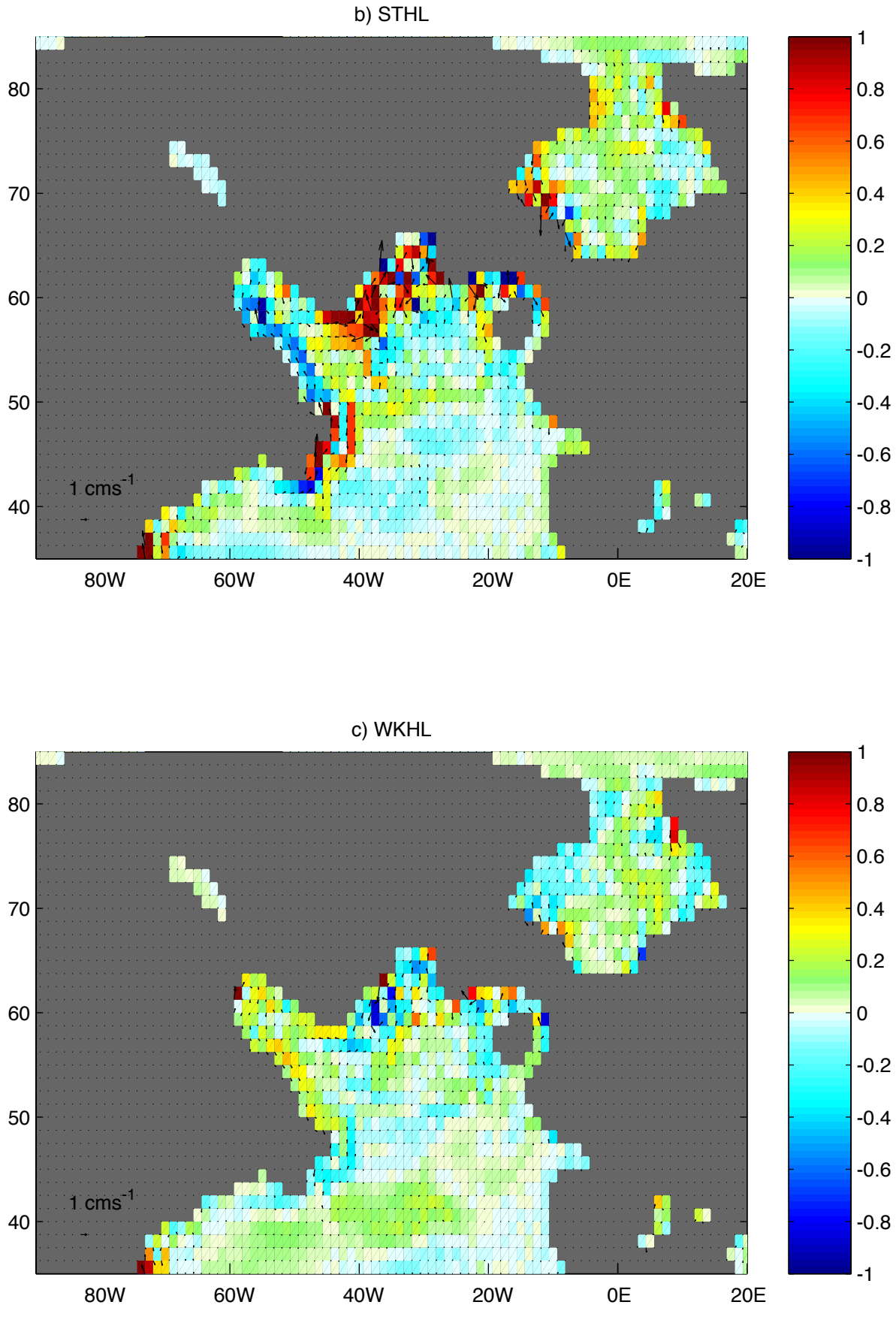

Fig. 12. HadCM3 1500m layer currents (cm s^{-1}), b) anomalous flow for STHL and c) anomalous flow for WKHL.

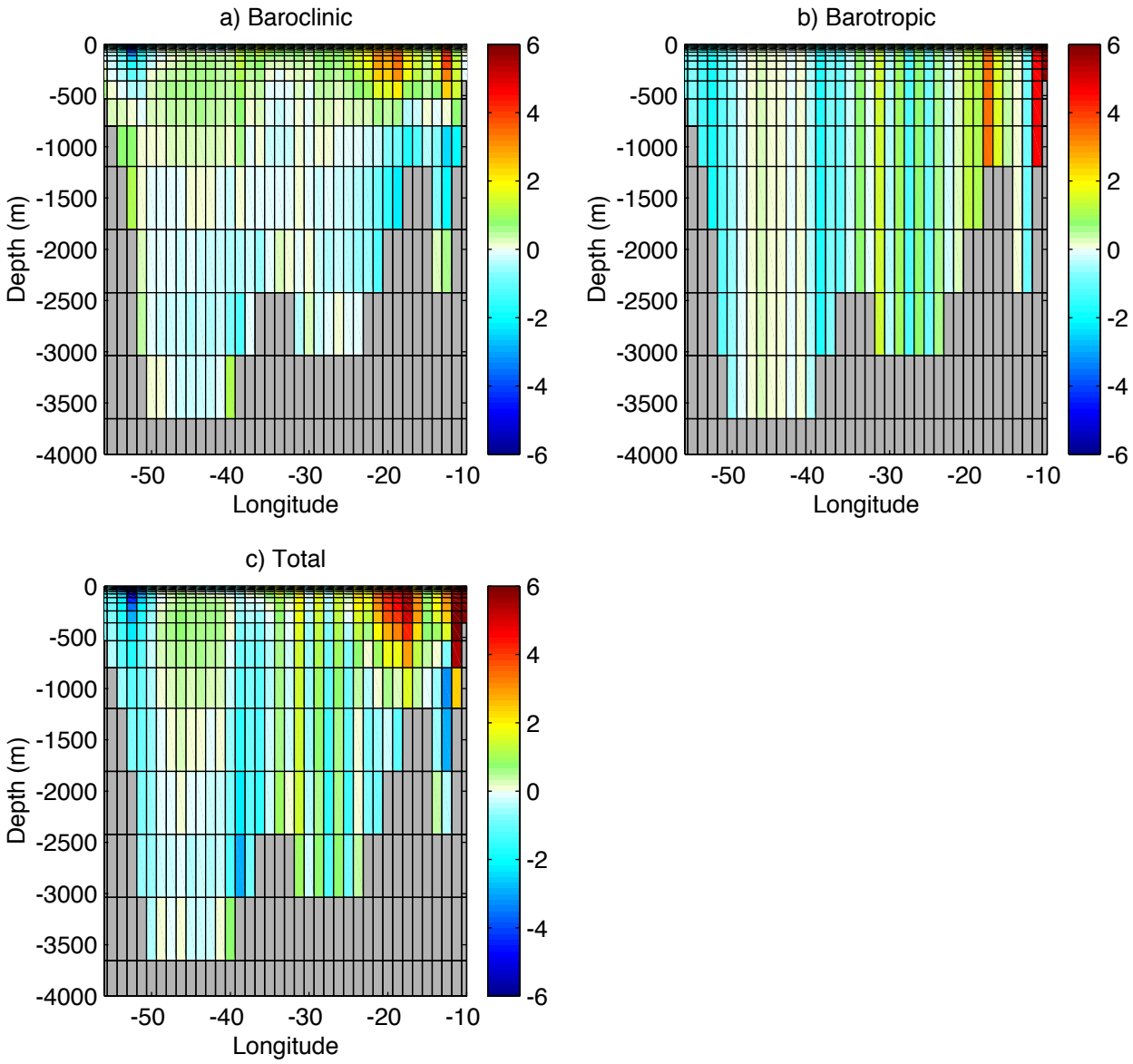

Fig. 13. Mean meridional flow (cm s^{-1}) across the 55^{o} N, Newfoundland to Ireland section (NFIR) for a) baroclinic flow, b) barotropic flow and c) total flow, for the period 2350-2449.

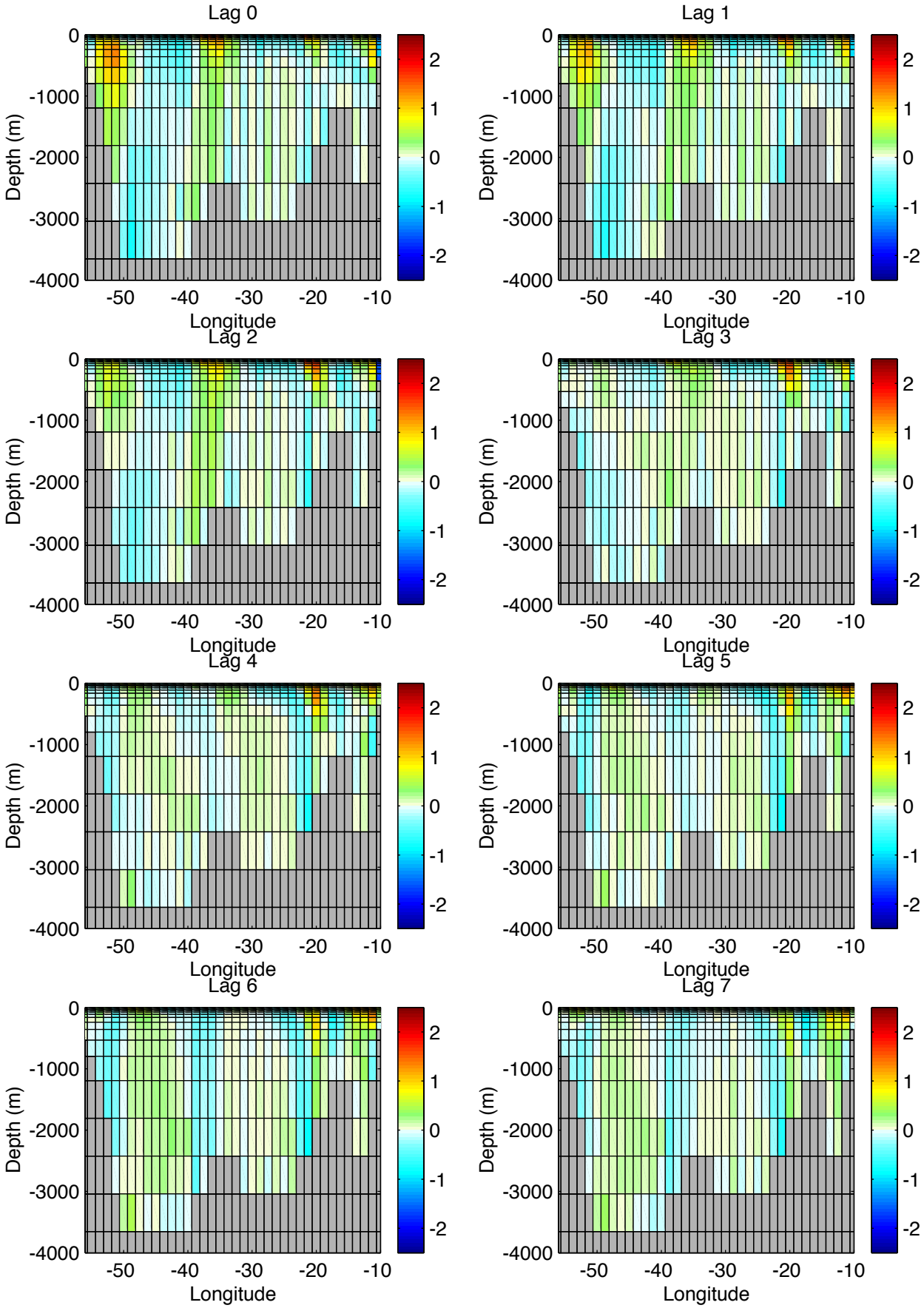

Fig. 14. Anomalous total flow (cm s^{-1}) across 55^{o} N, Newfoundland to Ireland (NFIR) at lags of 0 to 7 years relative to the set of STHL years.

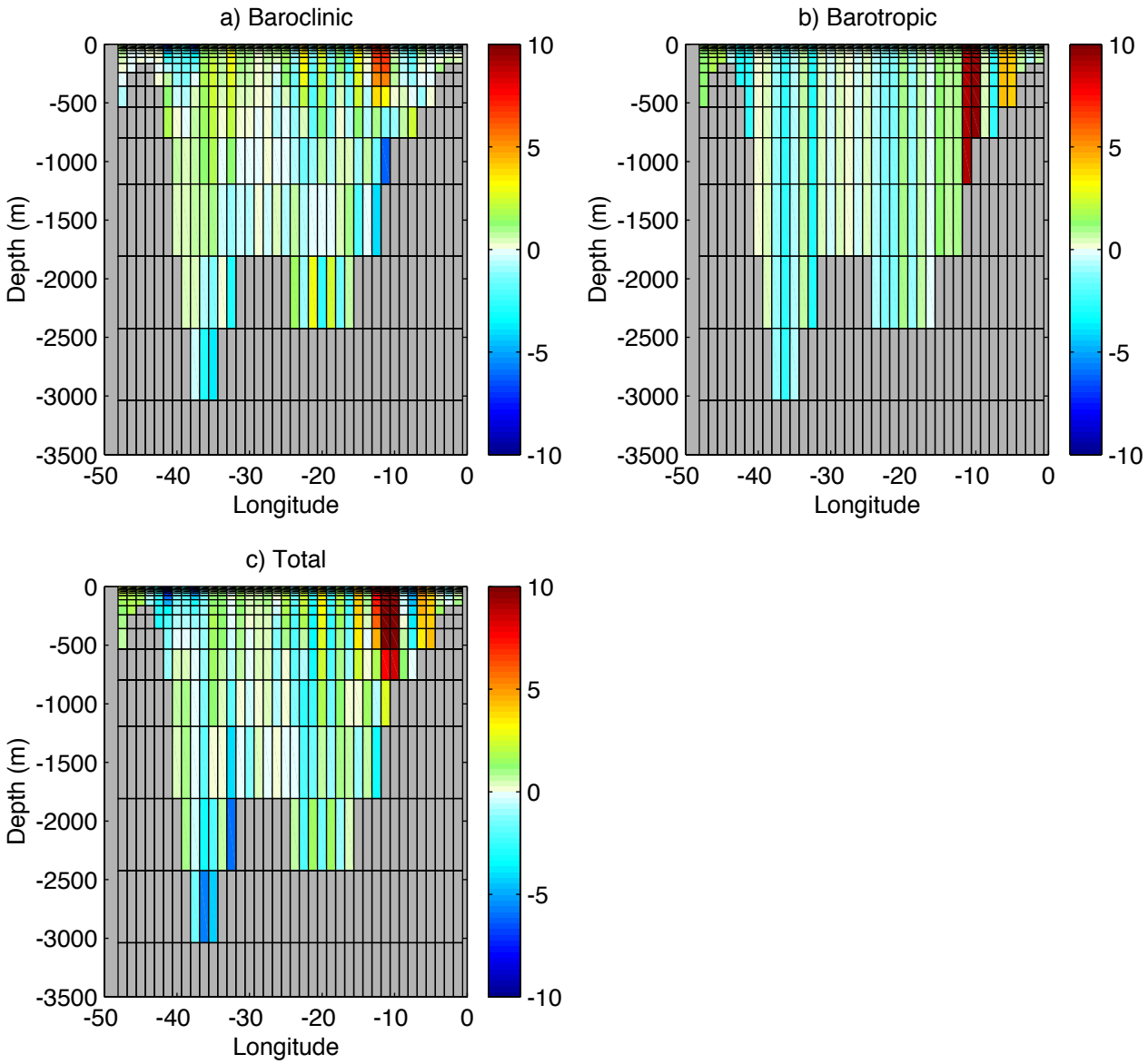

Fig. 15. Mean meridional flow (cm s^{-1}) across the 60^{o} N, Greenland to Scotland section (GS60) for a) baroclinic flow, b) barotropic flow and c) total flow, for the period 2350-2499.

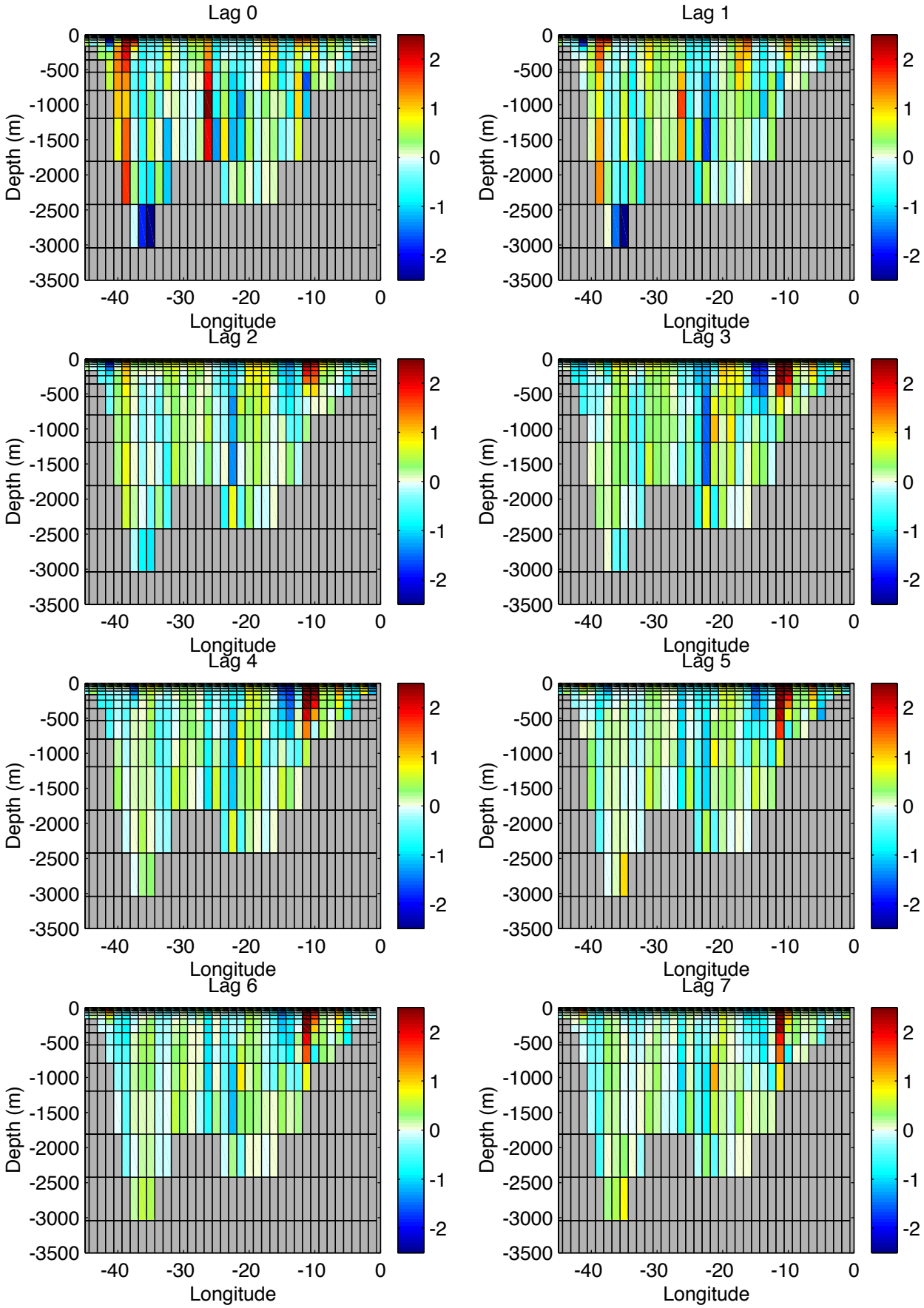

Fig. 16. Anomalous total flow (cm s^{-1}) across 60° N, Greenland to Scotland (GS60) at lags of 0 to 7 years relative to the set of STHL years.

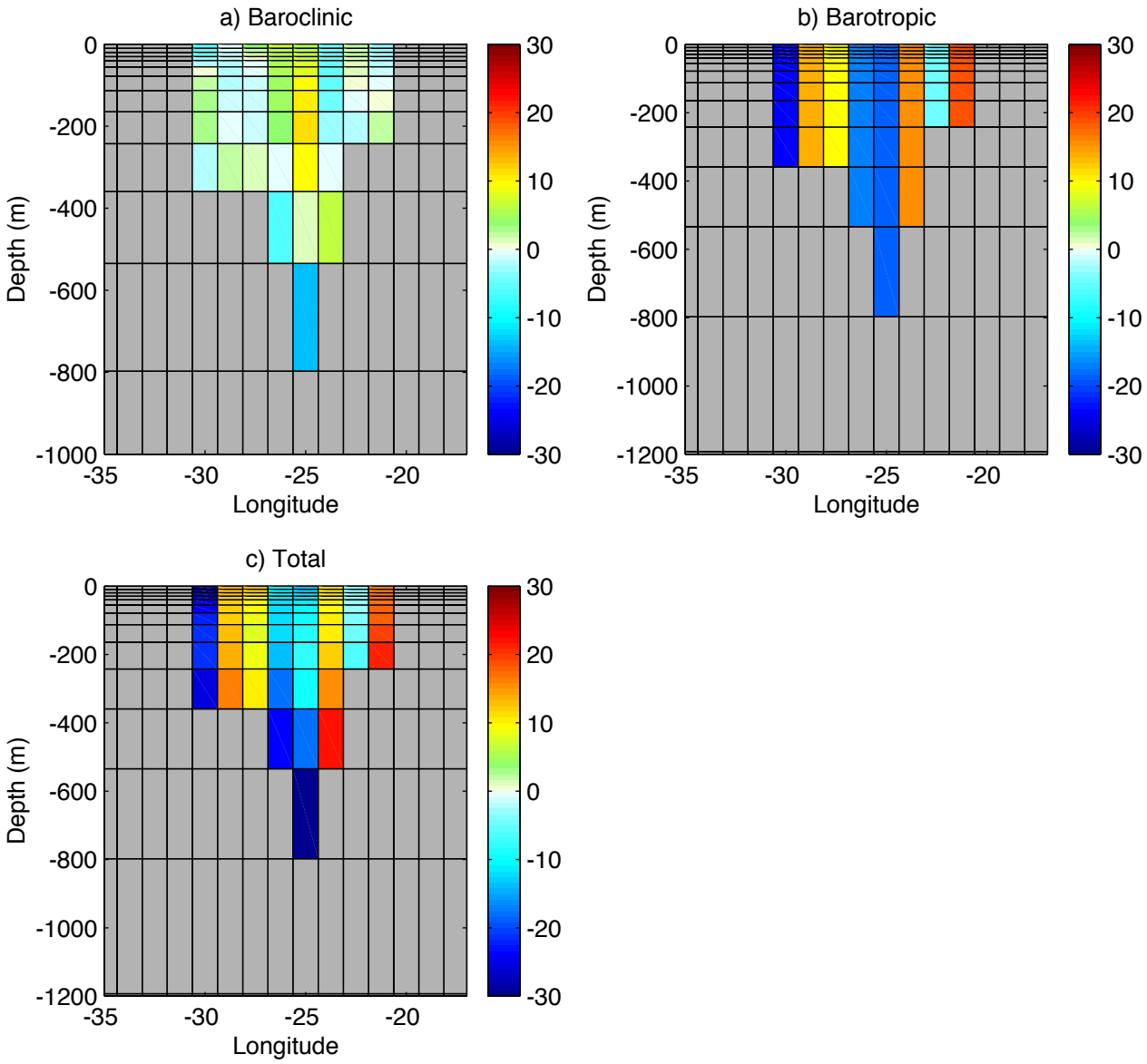

Fig. 17. Mean meridional flow (cm s^{-1}) across the Denmark Strait section (DMST) for a) baroclinic flow, b) barotropic flow and c) total flow, for the period 2350-2449.

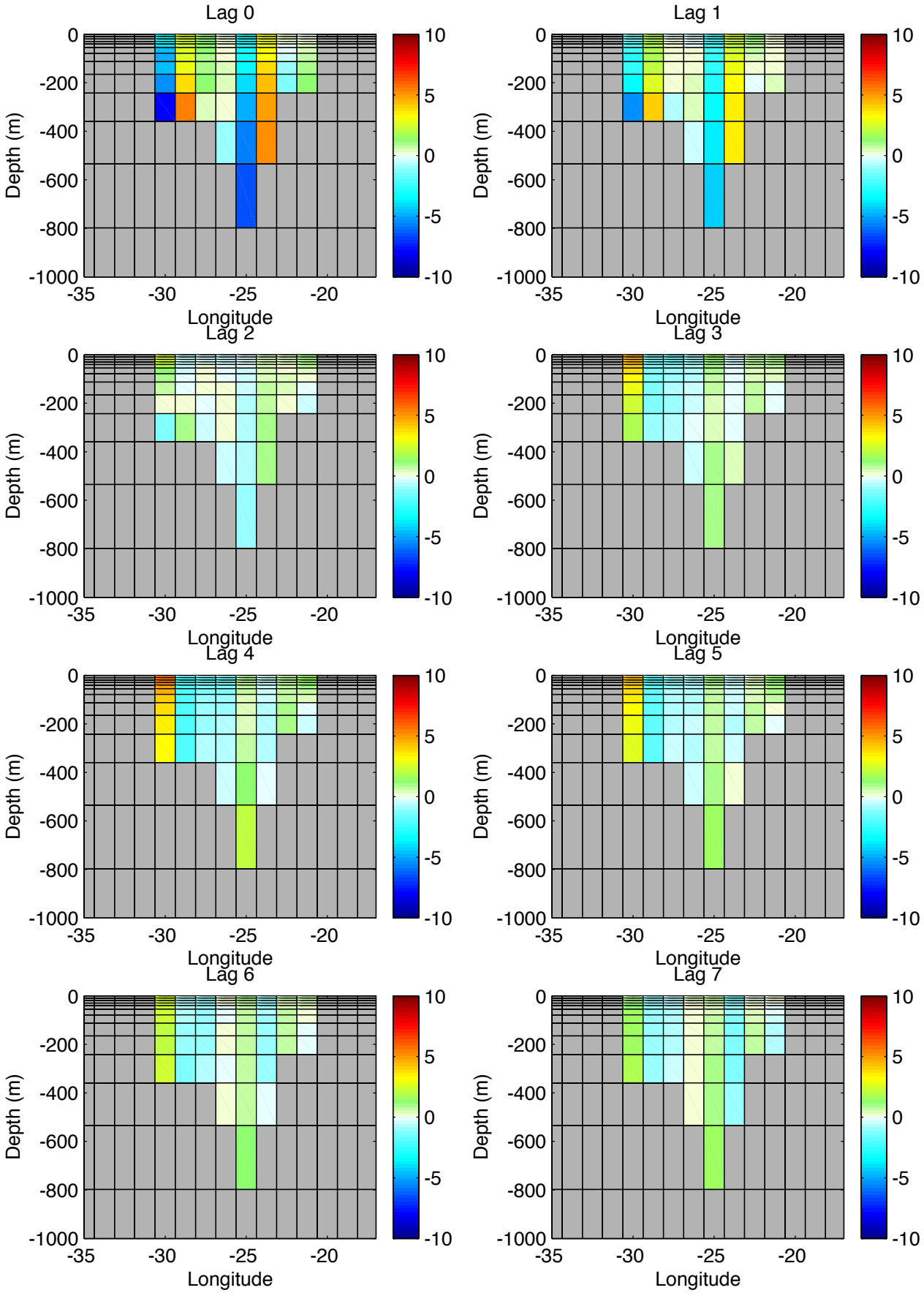

Fig. 18. Anomalous total flow (cm s^{-1}) across the Denmark Strait (DMST) at lags 0 to 7 years relative to the set of STHL years.

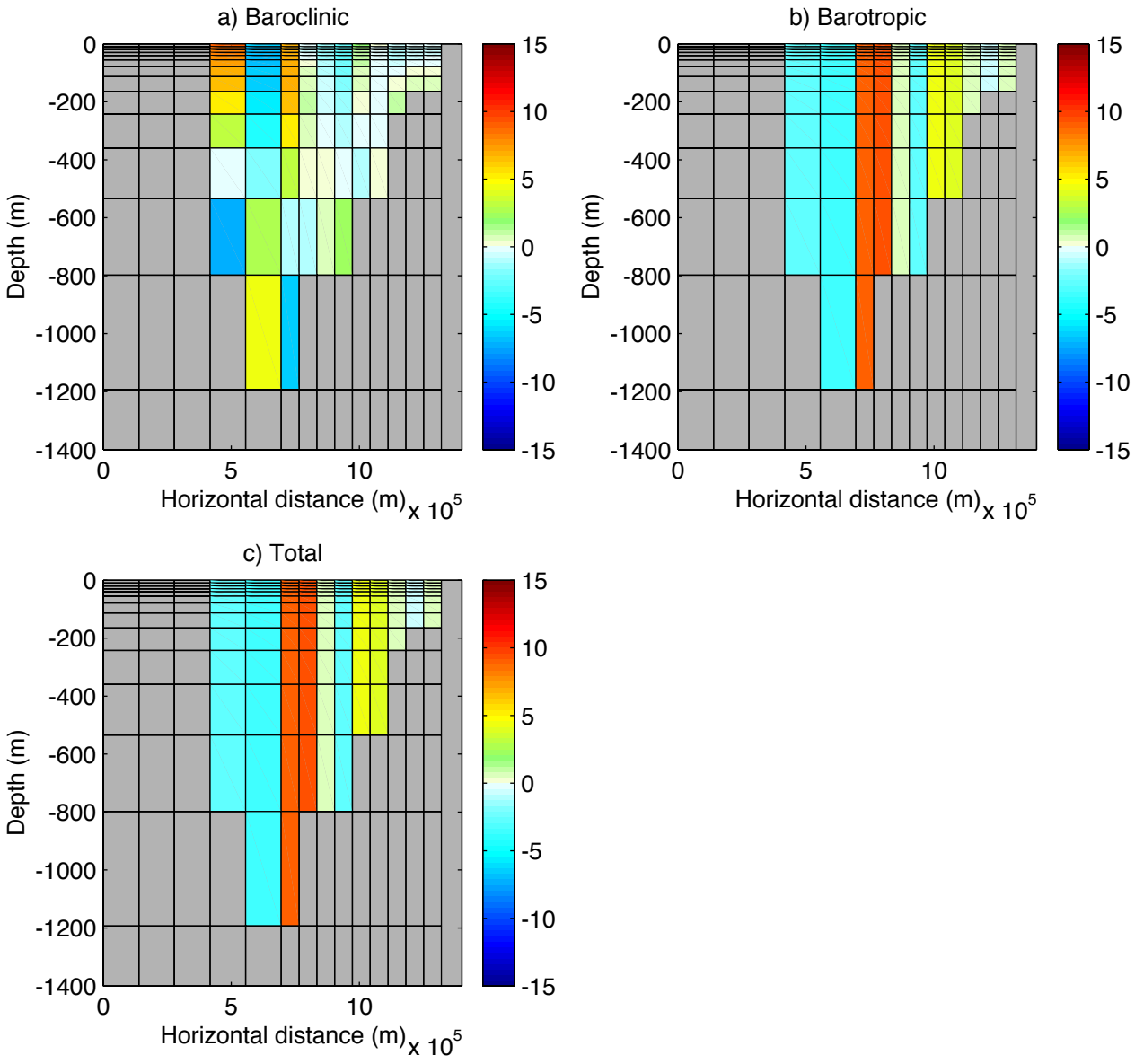

Fig. 19. Mean meridional flow (cm s^{-1}) across the Iceland Scotland Ridge (ISR) section for a) baroclinic flow, b) barotropic flow and c) total flow, for the period 2350-2449.

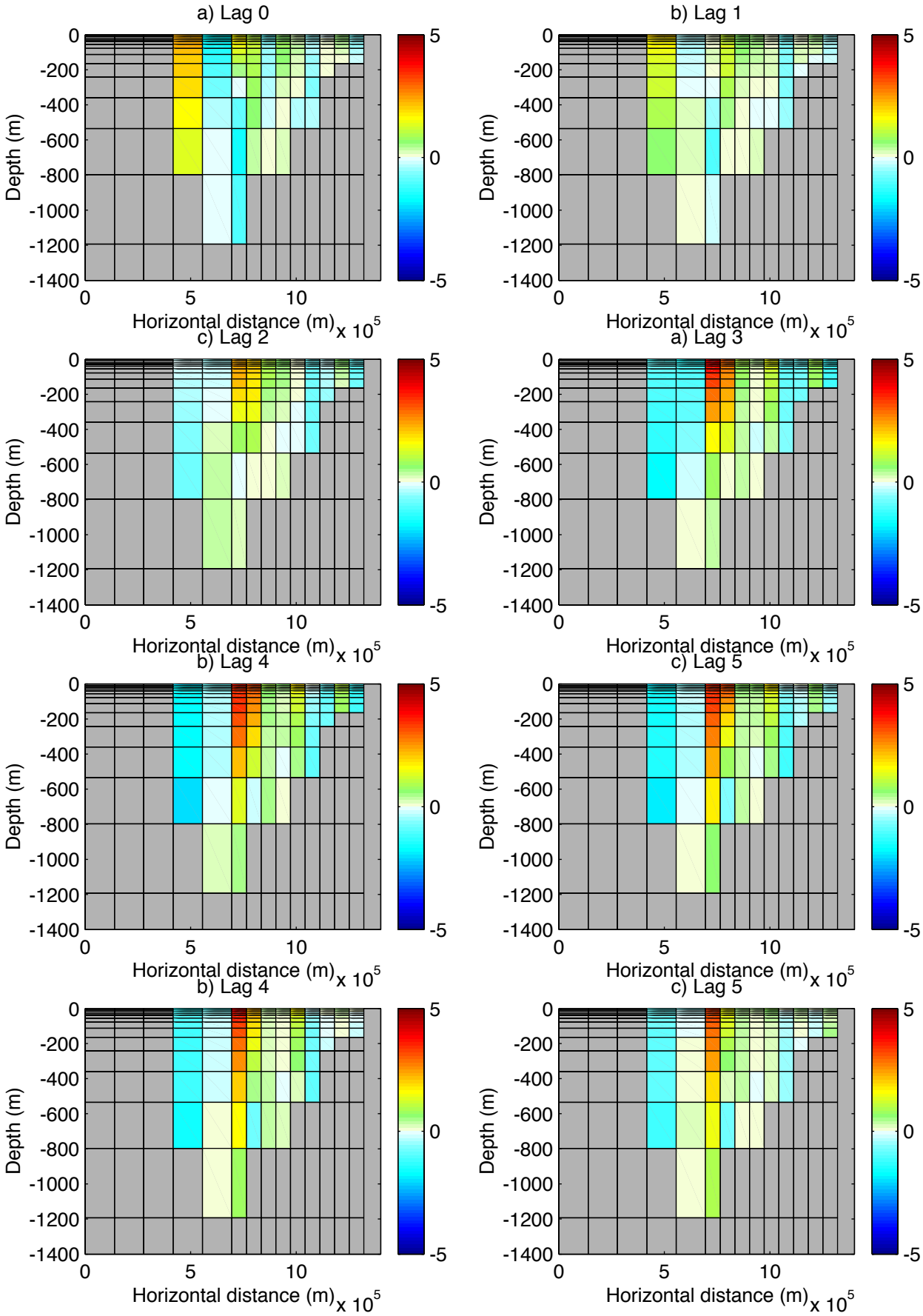

Fig. 20. Anomalous total flow (cm s^{-1}) across the Iceland Scotland Ridge (ISR) at lags 0 to 7 years relative to the set of STHL years.